Review of the role of surfactant dynamics in drop microfluidics

Kovalchuk, Nina M.; Simmons, Mark J.h.

DOI:
10.1016/j.cis.2023.102844

Document Version
Publisher's PDF, also known as Version of record

Citation for published version (Harvard):
Kovalchuk, NM & Simmons, MJH 2023, 'Review of the role of surfactant dynamics in drop microfluidics', *Advances in Colloid and Interface Science*, vol. 312, 102844. https://doi.org/10.1016/j.cis.2023.102844

Advances in Colloid and Interface Science 312 (2023) 102844

Contents lists available at ScienceDirect

Advances in Colloid and Interface Science

journal homepage: www.elsevier.com/locate/cis

Historical perspective

Review of the role of surfactant dynamics in drop microfluidics

Nina M. Kovalchuk *, Mark J.H. Simmons

School of Chemical Engineering, University of Birmingham, Edgbaston, Birmingham B15 2TT, UK

ARTICLE INFO

Keywords:
Microfluidics
Drop formation
Drop coalescence
Drop deformation
Surfactant adsorption kinetics
Microfluidic tensiometry

ABSTRACT

Surfactants are employed in microfluidic systems not just for drop stabilisation, but also to study local phenomena in industrial processes. On the scale of a single drop, these include foaming, emulsification and stability of foams and emulsions using statistically significant ensembles of bubbles or drops respectively. In addition, surfactants are often a part of a formulation in microfluidic drop reactors. In all these applications, surfactant dynamics play a crucial role and need to be accounted for. In this review, the effect of surfactant dynamics is considered on the level of standard microfluidic operations: drop formation, movement in channels and coalescence, but also on a more general level, considering the mechanisms controlling surfactant adsorption on time- and length-scales characteristic of microfluidics. Some examples of relevant calculations are provided. The advantages and challenges of the use of microfluidics to measure dynamic interfacial tension at short time-scales are discussed.

1. Introduction

The technology of drop microfluidics attracts a growing interest caused by its many possible novel applications to multiple areas of science and engineering. It enables formation of monodisperse drops over a broad range of sizes (10–1000 μm) and frequencies (1 Hz - 10 kHz) and their manipulation in a controlled manner.

The range of possible drop sizes are representative of those in emulsions. Drops of dispersed phase are separated by an immiscible continuous phase, the right choice of which prevents cross-contamination between the drop contents. This gives the possibility for drops to be used as independent reactors in such applications as analysis (in broad sense) and synthesis, as well as delivery vehicles. The advantages of microfluidic drop reactors are large area to volume ratio, small diffusion distances, uniform temperature, small hydrodynamic dispersion, highly reproducible flow and mixing patterns and the possibility of statistical analysis on large ensembles using small amounts of materials.

Microfluidics thus offer a broad range of configurations for analysis of emulsion stability, for example via the temporal evolution of drop ensembles under diverse hydrodynamic conditions [1–5] and analysis of the behaviour of pairs of drops in various flow configurations [6–8]. It also enables study of formation of crystal-like structures from drops or particles [9]. A thorough discussion on microfluidic studies of emulsions is provided in a recently published review [10].

Microfluidic drops are used for the study of polymer/protein phase behaviour and crystallisation [11] as well as reaction kinetics [11], enzyme studies [12] and various biomedical reactions [13]. Another

Abbreviations: A, surface area; b, adsorption constant in Langmuir isotherm; c, surfactant concentration (time and co-ordinate dependent); c_0, constant surfactant concentration far from interface; Ca, capillary number; CMC, critical micelle concentration; CTAB, hexadecyltrimethylammonium bromide (cetyltrimethylammonium bromide); D, diffusion coefficient; D^*, apparent diffusion coefficient for concentrations above CMC; DIT, dynamic interfacial tension; DTAB, dodecyltrimethylammonium bromide; F_D, viscous drag force; F_{IT}, interfacial tension force; G, elongational or shear rate; H, channel height; h_D, characteristic diffusion length-scale (thickness of depletion layer); IT, interfacial tension; γ, interfacial tension; k, fitting coefficients in various models; k_a, adsorption coefficient; k_d, desorption coefficient; L, characteristic length scale, drop length; P, pressure; P_d, dynamic pressure loss; P_c, capillary pressure; Pe, Peclet number; Q_d, flow rate of dispersed phase; Q_c, flow rate of continuous phase; R, drop radius ot radius of curvature; SDS, sodium dodecyl sulfate; t, time; t_D, characteristic adsorption time for diffusion-limited adsorption; t_{Dv}, characteristic equilibration time for deformed interface (diffusion-controlled kinetics); t_k, characteristic kinetic (adsorption/desorption limited) timescale; t_{Ma}, characteristic time of Marangoni flow; U, characteristic velocity; u_c, average velocity of continuous phase; u_d, velocity of dispersed phase; W, channel width; We, Weber number; Γ, surfactant adsorption (surface concentration); Γ_∞, limiting adsorption; δ, thickness of the diffusion boundary layer; ε_a, adsorption energy; ε_d, desorption energy; θ, polar angle; λ, viscosity ratio between dispersed and continuous phase; μ_c, viscosity of continuous phase; μ_d, viscosity of dispersed phase; ρ, density.

* Corresponding author.
E-mail address: n.kovalchuk@bham.ac.uk (N.M. Kovalchuk).

https://doi.org/10.1016/j.cis.2023.102844
Received in revised form 13 January 2023;
Available online 18 January 2023

branch of microfluidic analysis is for cell or microorganism assays, where one or several cells can be encapsulated in microfluidic aqueous drops of a required composition. The volume of the drop compartments can be reduced to less than one thousandth of that used for microtiter-plate-based assays considerably reducing material consumption. Drops containing cells can be stored for days before screening [14]. The number of cells in each drop can be adjusted either by changing the initial cell concentration in the dispersed phase or by diluting the dispersed phase before drop formation [14]. Drop microfluidics have been applied for single cell analysis [15] and to study cell-cell interaction on the individual cell level [16] including cytotoxicity assays [17] as well as cells' sensitivity to drugs [18].

The same technology can also be used for cell delivery. Drops of aqueous phase can be cross-linked and the resulting micro-particles with encapsulated cells are used in tissue engineering [19]. Solidified on-chip drops can be used in the pharmaceutical [20–22] and food [11] industries for drug, flavour and nutrients encapsulation.

Microfluidic drop reactors have also been broadly applied in chemical synthesis [23] including organic synthesis [24], formation of calcium phosphate particles for bone repair and regeneration [25] and creation of hydrogel microparticles [26,27], catalyst particles [28], quantum dots [29] and silver nanoparticles for various applications [30].

In many of these applications, surfactants are present in the dispersed and/or continuous phase as part of formulation or for drop stabilisation against coalescence. The presence of surfactants has implications in terms of interfacial dynamics which can affect various processes in drop microfluidics significantly. Dynamic interfacial tension defines the regime of drop formation, their size and size distribution, including number and size of satellite drops. A surfactant can change the hydrodynamic resistance of the multiphase flow in the channels containing drops/bubbles and therefore the flow distribution at junctions [31]. Surfactants affect drop deformability, including the relative deformability of core and shell in double emulsions [32]. Adsorbed surfactant often affects flow patterns inside the drops [33], which are crucial for performance of microfluidic reactors defining mixing intensity and shear stresses on encapsulated objects including living cells. It should be noted that large shear stresses can be injurious and even deadly for some types of cells [34,35]. Surfactant presence and distribution on the drop surface is detrimental for probability of drop coalescence [1,7,36], flow patterns and mixing after coalescence [6,37,38].

This review paper is thus focused on the effect of surfactant and its dynamic on microfluidic processes. The paper is organised as follows. Section 2 provides a general overview of surfactant dynamic effects. Section 3 considers the main types of microfluidic drop generators and the effect of surfactant on drop formation. Section 4 is devoted to the effect of surfactant on drop movement in micro-channels. The coalescence of surfactant-laden and surfactant-free drops is considered in section 5, which is followed by microfluidic methods for measurement of dynamic interfacial tension on short time-scales in section 6. Conclusions and outline of future work are given in section 7.

2. Dynamic surfactant effects

When a new interface is created from a surfactant solution, initially it is clean and the value of interfacial tension is equal to that of a pure solvent. A gradual surfactant adsorption from the bulk liquid onto the interface results in a decrease of interfacial tension down to an equilibrium value. This time-dependent interfacial tension is called the dynamic interfacial tension, DIT. The change of interfacial tension/quantity of surfactant present on the interface can be controlled by the rate limiting step of either the rate of surfactant mass transfer from the bulk to close to the interface or by the rate of adsorption of surfactant molecules close to the interface onto the interface (and adapting to the equilibrium configuration at the interface). If convection in the liquid can be neglected and diffusion is the only mechanism of mass transfer, then the diffusion controlled adsorption, Γ, at the initially clean interface is described by Ward-Tordai equation [39], which for spherical interface of radius R reads as [40,41].

$$\Gamma(t) = \sqrt{\frac{4D}{\pi}}\left[c_0\sqrt{t} - \int_0^{\sqrt{t}} c(t-\tau)d\left(\sqrt{\tau}\right)\right] \pm \frac{D}{R}\left[c_0 t + \int_0^t c(\tau)d\tau\right] \quad (1)$$

Where "+" corresponds to the surfactant transfer from the outside of the drop and "–"corresponds to the surfactant transfer from the inside of the drop. The surfactant is assumed to be soluble only in one phase, i.e. no mass transfer through the interface is considered. Eq. (1) shows that adsorption is the fastest when it occurs on a curved convex interface (i.e. from outside a drop) and the rate increases with a decrease of the drop radius. This faster adsorption is due to increased volume of surfactant solution adjacent to the curved drop surface outside of the drop when compared to the flat interface. If the diffusion is from the inside of drop, the adjacent volume is smaller than for the flat surface and the adsorption rate is slower.

For the short time approximation:

$$\Gamma(t) = c_0\left(\sqrt{\frac{4Dt}{\pi}} \pm \frac{D}{R}t\right) \quad (1a)$$

In Eqs. 1 – 1a c_0 is the constant bulk concentration of surfactant far from the interface, c is the time dependent sub-surface concentration and D is surfactant bulk diffusion coefficient. Note, Eq. (1) describes surfactant transfer from the large volume of liquid where concentration far from the interface remains constant. The situation becomes complicated when the liquid volume is small and surfactant depletion occurs. This can happen during adsorption from the thin liquid film between drops prior to coalescence or during adsorption from the volume of a small drop to its surface, as will be discussed below. Detailed discussion on the Ward-Tordai equation and its approximations and application is given in [42,43].

In the case of kinetics controlled by mass transfer there is always a local equilibrium between $\Gamma(t)$ and $c(t)$ described by adsorption isotherm, the simplest of which is the Langmuir isotherm

$$\Gamma = \Gamma_\infty \frac{bc}{1+bc} \quad (2)$$

where Γ_∞ is the limiting adsorption and b is the adsorption constant, accounting for surfactant activity. To describe adsorption process more precisely, more sophisticated isotherms taking into account interactions between adsorbed molecules, compressibility of adsorption layer, various orientation of molecules at the interface or adsorption of surfactant mixtures are used, see for example [44] and references herein. Note, the adsorption corresponding to the equilibrium interfacial tension is described by Eq. (2) with $c = c_0$ since there is no longer a concentration gradient between sub-surface and the bulk.

An important parameter related to dynamic interfacial tension is the characteristic adsorption time after which equilibrium interfacial tension is reached. For diffusion-limited adsorption, an equation for an estimation of this time, t_D, is based on a simple mass balance [45–47]. The characteristic diffusion length-scale or, in other words, depletion depth, h_D, is introduced as the depth of solution which should be depleted to supply the flat interface with the required amount of adsorbed surfactant:

$$h_D = \frac{\Gamma}{c_0} \quad (3)$$

The characteristic adsorption time is then defined as [45].

$$t_D = \frac{h_D^2}{D} = \frac{\Gamma^2}{c_0^2 D} \quad (4)$$

Using the Langmuir adsorption isotherm this gives

$$t_D = \frac{1}{D}\left(\frac{\Gamma_\infty b}{(1+bc_0)}\right)^2 \tag{4a}$$

Eq. (4a) shows that the surfactant adsorption time can vary over a broad range. Diffusion coefficients and values of Γ_∞ are rather similar for most of low molecular weight surfactants, but the adsorption constant, *b,* accounting for surfactant activity and c_0 can change over several orders of magnitude [48]. The minimum surface tension is observed at maximum concentration of monomers, c_{max}, being equal to the solubility limit or to critical micelle concentration (CMC) for micellar surfactant solutions. A noticeable change in interfacial tension when compared to the pure solvent is observed at concentrations $c_{min} \sim 5 \times 10^{-5}$ - 5×10^{-2} CMC depending on the type of surfactant [48]. For typical non-ionic surfactants, which do not form micelles, and ionic surfactants $bc_{max} =$ O(1) and $bc_{min} << 1$ [48]. Therefore, for these $t_D \sim b^2$ and can vary over 4 orders of magnitude. The larger the value of b, the larger is the characteristic adsorption time. For typical non-ionic micellar surfactants $bc_{max} >> 1$ and $bc_{min} =$ O(1) [48]. Therefore, for these surfactants, $t_D \sim CMC^{-2}$ for concentrations close to CMC and $t_D \sim b^2$ at small concentrations.

An increase of the characteristic adsorption time with an increase of surfactant activity has a simple explanation: a larger activity means larger partition coefficient between the interface and bulk phase, i.e. the amount of adsorbed surfactant increases with an increase of activity at the same bulk concentration. To supply that larger amount of surfactant, a larger volume of adjacent solution has to be depleted. Thus, the larger activity corresponds to a larger depletion depth and therefore to a larger adsorption time.

Eqs. (2)–(4) are valid only for concentrations below the CMC. Above it, the bulk concentration of monomers and therefore adsorption remains constant, due to thermodynamic equilibrium between adsorbed molecules and bulk monomers, whereas micelles provide an additional contribution to the surfactant transfer which can be accounted for by replacing the monomer diffusion coefficient, *D*, by apparent diffusion coefficient D^* [43].

$$D^* = D(1+\beta)\left(1+\beta n^{-1/3}\right) \tag{5}$$

where $\beta = (c_0 - CMC)/CMC$ and *n* is the micelle aggregation number.

Typical values of characteristic adsorption time for diffusion-controlled adsorption are considerably larger for non-ionic surfactants than for ionic ones due to their larger activity and smaller CMC. For example, based on data provided in [48] $t_D \sim$ 400 ms for diffusion controlled adsorption of the non-ionic surfactant Triton X-100 (diffusion coefficient $D = 3.2 \cdot 10^{-10}$ m^2/s [48]), but $t_D \sim$ 0.9 ms for the ionic surfactant sodium dodecyl sulphate (SDS, $D = 6.4 \cdot 10^{-10}$ m^2/s [49]), both at the CMC. The typical time of drop formation in microfluidics is in the range of 1–100 ms, therefore it can be expected that SDS will reach the equilibrium interfacial tension on the time scale of drop formation, whereas Triton X-100 will not. It should be noted that the characteristic diffusion length scale for SDS is around 0.8 μm, which is much smaller than the typical size of microfluidic drops (100 μm). Therefore, the drop interface can be considered as flat and Eqs. (3), (4) are valid. The characteristic diffusion length scale for Triton X-100 is around 11 μm, thus is comparable with drop radius and therefore the surface curvature should be taken into account, especially for drops with $R < 100$ μm.

The effect of surface curvature, which may be of importance for the microfluidic drops, was considered in [50] by developing further the approach suggested in [45]. If the surfactant is dissolved in the continuous phase (diffusion from outside the drop) then the characteristic depletion length scale for a spherical drop of radius R is

$$h_{DRc} = R\left[\left(\frac{3\Gamma}{Rc_0}+1\right)^{1/3} - 1\right] \tag{6}$$

It is easy to recalculate data from the previous paragraph using Eq. 6 and obtain the characteristic diffusion timescale for adsorption from the continuous phase to the drop of radius of 50 μm. This results in values of ~0.9 ms for SDS and ~ 280 ms for Triton X-100. As expected from discussion in the previous paragraph, the characteristic diffusion timescale for SDS remains the same as calculated using a flat interface approximation. However, the characteristic adsorption time of Triton X-100 decreases considerably for adsorption to the drop surface from the continuous phase. It decreases further to 130 ms at drop radius of 10 μm. Note, other than Eq. (6), characteristic length scales are possible for diffusion to spherical interface, see discussion in [50] and references herein.

The situation becomes even more interesting if surfactant is dissolved in the dispersed phase. Using the same approach as [45,50] it is easy to determine the characteristic depletion length scale as

$$h_{DRd} = R\left[1 - \left(1 - \frac{3\Gamma}{Rc_0}\right)^{1/3}\right] \tag{7}$$

Calculations show that, for adsorption of SDS from a drop of radius 50 μm, the characteristic depletion length scale is around 0.9 μm, and characteristic time scale is around 1.2 ms, i.e. both are only slightly larger than for the flat interface. For Triton X-100, the characteristic diffusion time scale increases nearly twice in comparison to the flat interface, to 790 ms and characteristic depletion length scale, 16 μm is comparable to the drop radius. The latter means that adsorption will result in a considerable depletion of surfactant from the bulk phase and the equilibrium interfacial tension should be considerably larger than expected for the initial bulk concentration. Thus, if a surfactant is dissolved in the dispersed phase, the characteristic depletion length scale is to be always calculated and if the condition $h_{DRd} << R$ is not fulfilled, a surfactant mass balance is required to find the equilibrium bulk concentration and equilibrium interfacial tension.

A number of non-ionic surfactants can be soluble in both the continuous and dispersed phase. In this case equilibrium concentration and equilibrium interfacial tension depend on surfactant partition coefficient. Partition should be also taken into account for calculation of characteristic adsorption time.

Dynamic surfactant effects can reveal themselves not only during formation of a new interface, but also during deformation of an interface including one at equilibrium surfactant adsorption. In microfluidics, this happens during the drop movement within a channel, when passing through restrictions and junctions or during drop coalescence [6,33,51]. Strong deformations accompany neck dynamics close to pinch-off [52]. Deformations can result in non-uniform surfactant distributions forming surface tension gradients known as Marangoni stresses. These can lead to surface retardation up to complete immobilisation, with the well-known example being the retardation of the surface of a rising bubble, which demonstrates a terminal velocity similar to a hard sphere [53,54]. For microfluidic drops, surface immobilisation will retard the recirculation inside the drop during its formation and suppress completely any recirculation and mixing within the drops moving through the channels.

The response of surfactant-laden interfaces to expansion/contraction is characterised by dilational surface viscoelasticity [55]. Similar to dynamic interfacial tension, dilational surface viscoelasticity depends on drop size and transfer direction (surfactant in continuous or dispersed phase) [56].

When a drop with an adsorbed surfactant deforms, the equilibrium between the bulk and interface is violated and a certain time is required to restore it. For a flat interface, the characteristic equilibration time for diffusion-controlled kinetics is given by [57].

$$t_{Dv} = \frac{4\pi}{D}\left(\frac{d\Gamma}{dc}\right)^2 \tag{8}$$

which for the case of Langmuir isotherm can be rewritten as

$$t_{Dv} = \frac{4\pi}{D}\left(\frac{\Gamma_\infty b}{(1+bc_0)^2}\right)^2 \tag{8a}$$

Comparison of this characteristic time with the characteristic time of surface deformation shows the importance of Marangoni phenomena for the situation under consideration. If surface deformation is much faster than the surfactant equilibration, the surfactant behaves as an insoluble one and can produce a noticeable Marangoni stress.

Marangoni stress applies to the interface and violates continuity of the viscous stress at the interface [58]. It affects the surface flow and can result in full surface retardation. At an initially motionless interface, Marangoni stress causes surface flow in the direction of higher interfacial tension tending to reduce interfacial tension gradient. This influences the flow in both continuous and disperse bulk phases and therefore its characteristic time scale depends on both bulk viscosities as [6].

$$t_{Ma} = \frac{\mu_c + \mu_d}{\Delta\gamma/L} \tag{9}$$

where $\Delta\gamma/L$ is interfacial tension gradient. In the case of interfacial tension gradient caused by surface deformation, τ_{Ma} shows to which extent Marangoni flow can reduce this gradient. Eq. (9) shows that gradients are larger when continuous and disperse phase are more viscous. Note, the viscosity of the surfactant-laden phase is implicitly included in Eq. (8) as well, because the surfactant diffusion coefficient is inversely proportional to viscosity. Therefore, it can be expected that Marangoni phenomena are more pronounced when the surfactant-laden phase has high viscosity.

Both eqs. (4) and (8) for characteristic time assume that diffusion is the main mechanism of surfactant mass transfer, i.e. convective mass transfer is negligible. This is often not the case in microfluidics where convection is present within both continuous and dispersed phases. The importance of convective mass transfer is reflected by Peclet number

$$Pe = \frac{UL}{D} \tag{10}$$

where U is the characteristic velocity, L is the characteristic length scale, for example drop radius, R, and D is diffusion coefficient. If $Pe << 1$, contribution of convection into mass transfer can be neglected, otherwise convection is important and diffusion mass transfer is limited to diffusion (concentration) boundary layer close to the interface. The choice of U in Eq. (10) depends on the type of mass transfer. For a drop formed in a continuous phase of surfactant solution, the velocity of the drop of dispersed phase relative to the continuous phase can be used. If the dispersed phase is surfactant-laden and continuous phase is surfactant-free, the average velocity of recirculation inside the drop is a most obvious choice. If surfactant is transferred from continuous phase to a Taylor drop moving in the channel, convection can contribute only to the mass-transfer to the front and rear part of it and the average recirculation velocity within a slug of continuous phase separating two drops can be used as a characteristic velocity. In the case of Taylor flows, surfactant transfer from the films between the drop and channel wall is purely diffusional.

The surface of a microfluidic drop in a surfactant-laden system can be either mobile or retarded. The latter occurs due to Marangoni stresses, which prevent interfacial motion. If surfactant is dissolved in the continuous phase, the thickness of the diffusion boundary layer around the spherical drop with retarded interface moving in liquid with relative velocity, U, can be calculated using the expression for boundary layer thickness, δ, around a solid particle moving in unbounded liquid [59].

$$\delta = f(\theta)\left(\frac{4DR^2}{3U}\right)^{1/3} = \frac{1.15\left(\theta - \frac{sin2\theta}{2}\right)^{1/3}}{sin\theta}\left(\frac{4DR^2}{3U}\right)^{1/3} \tag{11}$$

where θ is the polar angle (θ = 0 at the front of the particle and θ = π at the rear) and D is the surfactant diffusion coefficient. According to [59], the uncertainty in f(θ) at θ = 0 can be resolved as f(0) = 1. It follows from Eq. (6) that the thickness of diffusion layer is not uniform around the moving drop. It has minimum at the front of the drop and increases towards the rear. Formally f(π) = ∞, but Eq. (6) is valid only for δ << R. Nevertheless, the assumption of increase of the thickness of diffusion boundary layer from the front to the rear of drop is valid. Therefore, conditions for adsorption/desorption can be very different in different parts of the moving drop. Note, where the thickness of diffusion boundary layer is larger than the thickness of depletion layer, Eq. (3), the last is to be used for calculation of characteristic adsorption time of diffusion limited adsorption.

If the drop surface is mobile, then the thickness of diffusion boundary layer can be calculated as [59].

$$\delta = \sqrt{\frac{\pi RD}{3v_0}}\sqrt{\frac{2+cos\theta}{(1+cos\theta)^2}} \tag{12}$$

where

$$v_0 = \frac{\mu_c}{2}\frac{U}{\mu_c + \mu_d} \tag{13}$$

is the surface velocity of liquid at the drop equator and μ_c and μ_d are viscosities of continuous and dispersed phases respectively. Similarly to the case of retarded interface, the thickness of the diffusion boundary layer near the mobile interface has a minimum at the front of the drop and increases in the direction of rear. Note, Eqs. (11)–(13) were derived for a drop falling in a motionless continuous phase under gravity and give only a rough estimation of the thickness of diffusion boundary layer. In particular, the distance between the drops in microfluidic device is of the same order of magnitude as drop size, i.e. each drop is moving in the wake of a previous drop. This increases the thickness of diffusion boundary layer at the front of the drop. If the drop size is larger than the channel width, then the thickness of the boundary layer can be larger than the thickness of the thin film of continuous phase between the drop and the wall. The diffusion boundary layer can be thinner than the depletion depth if there is a considerable motion of the dispersed phase relative to the continuous phase.

For surfactant adsorption from inside the drop, there are recirculatory flow patterns inside the drop during the drop formation and movement inside the channel, which mix solution inside the drop. If the drop surface is retarded, then the recirculation in the separated moving drop is mainly suppressed. For a growing new drop, where there is an external pressure supporting movement of the dispersed phase, recirculation can be present even if the surface is retarded. In this case, the solution for the flow within a cylindrical pipe in the area where hydrodynamic boundary layer is fully developed, but the concentration boundary layer is still developing [59], can be used for a rough estimate

$$\delta = \frac{1}{0.67}\left(\frac{DRx}{v_0}\right)^{1/3} \tag{14}$$

where v_0 is the maximum velocity in the centre of pipe and x is the distance from the point of the flow entrance. For the flow in the drop with a retarded surface, the distance from the drop apex can be used as x and the maximum velocity of the flow inside the drop (relative to surface) can be used as v_0. Note, at $x = R$, Eq. (14) is rather similar to Eq. (11), therefore Eq. (12) at θ = 0 can be used as a rough estimation of the concentration boundary layer for a drop with mobile interface when the surfactant is in the dispersed phase. However, it should be stressed that these approximations are valid only if δ << L, where L is the drop size.

If the mass transfer rate is the same or even faster than adsorption/desorption itself, the kinetics is defined as mixed or adsorption/desorption controlled. A detailed discussion of the mechanisms behind adsorption/desorption controlled kinetics and experiments enabling its identification is given in [60,61]. In particular, it is stressed in [60] that

deviations from the diffusion kinetics, especially in the long time limit, are often not due to the presence of any adsorption barriers, but to the presence of impurities in surfactant solutions with larger activity but slower adsorption than the main component. It should be always taken into account that a high volumetric purity of surfactant does not necessarily imply surface-chemical purity [62], i.e. absence of very small concentrations of active surfactants. Another reason for apparent non diffusion limited kinetics can be the wrong choice of adsorption isotherm [50].

If adsorption/desorption is the rate determining step, then there is no equilibrium between the surface and sub-surface and instead of Eq. (2) the relation between the adsorption and concentration in the simplest case of Langmuir kinetics is

$$\frac{d\Gamma}{dt} = k_a c(\Gamma_\infty - \Gamma) - k_d\Gamma \tag{15}$$

where k_a and k_d are adsorption and desorption coefficient respectively. Eq. (15) turns into Eq. (2) at equilibrium, when $d\Gamma/dt = 0$, with $b = k_a/k_d$. Note that the adsorption and desorption coefficients are not always constant, but can depend on surfactant concentration. In this case, the Frumkin equation can be used instead of Langmuir Eq. (15) with $k_{a,d} = k^0_{a,d} exp\left(\varepsilon_{a,d}\left(\frac{\Gamma}{\Gamma_\infty}\right)^n\right)$. There are variations of Frumkin equation in practical use. In some cases, it is accepted that $n = 1$ assuming linear dependence of adsorption/desorption energy on surface concentration [61], in other cases it is accepted that $\varepsilon_a = 0$, see for example [63,64]. It is important, however, that the parameters found from dynamic measurements have to be in agreement with parameters of equilibrium Frumkin isotherm for the same surfactant.

The characteristic kinetic (adsorption/desorption limited) timescale related to Eq. (15) can be estimated as [47,50].

$$t_k = \frac{1}{k_a c + k_d} \tag{16}$$

Comparison of diffusion and kinetic time scales enables the determination of the rate limiting step in surfactant adsorption. However, such a comparison requires knowledge of adsorption and desorption coefficients, which are difficult to find with a high level of fidelity for common low molecular weight surfactants, because of the difficulty of reliable measurements on length and time scales where at least mixed kinetics takes place. As seen from Eqs. (5), (6), (11), (12), a decrease of the relative importance of diffusion mass transfer can be achieved by transfer from the outside to the surface of small drops, increase of surfactant concentration and/or intensification of convection. Therefore, microfluidics can be a useful tool for estimation of kinetic coefficients [64].

Some values of adsorption/desorption coefficients available in the literature are collected in Table 1. The most common surfactants for which these coefficients were found are non-ionic surfactants, in particular those with a polyethylene oxide hydrophilic part. There are some discrepancies in the values provided for the same surfactant by different authors. One of the reasons can be a difference in the chemical composition, since they are mixtures of several homologues. The Frumkin model was used for data analysis of alkyl polyethylene oxides, but it is well known that this class of surfactants is much better described by a model taking into account multiple adsorption states [65].

There are also discrepancies between data for the ionic surfactant sodium dodecyl sulphate, SDS. For ionic surfactants, diffusion limited kinetics was observed at short timescales, but some electrostatic barrier effects were observed at longer timescales due to the electrical potential of the adsorbed surfactant [66]. In the presence of salts, diffusion controlled kinetics was observed due to the screening of electrostatic interactions at high ionic strength [61]. It was suggested in [61] that earlier data on adsorption/desorption constants for ionic surfactants should be re-evaluated to take into account the non-homogeneity of the bulk concentration in the experiments performed. Therefore, further studies are required to obtain reliable values of adsorption and desorption coefficients, as well as criteria to enable the differences between diffusion and adsorption/desorption limited kinetics to be clearly identified.

If the surfactant characteristics are known, the criterion

$$\frac{k_d R}{D}\frac{\Gamma}{c_0} \ll 1 \tag{17}$$

has been put forward in [46] although without strong arguments to define the range of surfactant concentrations where adsorption-desorption kinetics is the rate limiting step. In particular, adsorption-desorption becomes more important when the drop radius, R, decreases, i.e. for microfluidic drops rather than macroscopic drops. Another simplified criterion to estimate the relative importance of mass transfer and adsorption kinetics on surfactant dynamics was suggested in [47], where a characteristic length scale $R_{D\text{-}K}$ was introduced as

$$R_{D-K} = \frac{D}{k_a \Gamma_\infty} \tag{18}$$

If the drop radius $R << R_{D\text{-}K}$, surfactant dynamics are controlled by adsorption/desorption kinetics, whereas they are diffusion controlled for $R >> R_{D\text{-}K}$. Eqs. (17), (18) were derived for surfactant adsorption from the continuous phase and cannot be used for surfactant adsorption from the dispersed phase, because of the different equation for characteristic depletion length scale. In this latter case, the adsorption time

Table 1
Available values of adsorption and desorption coefficients. For the Frumkin model k^0_a and k^0_d are provided. The additional parameters for the Frumkin model can be found in the listed references.

Surfactant	Solvent	2nd phase	Model	k_a, m^3/mol/s	k_d, 1/s	Ref.
SDS	Water	Air	Langmuir	0.64	5.87	[67]
SDS	Water	Air	Langmuir	44.8	92	[68]
$C_{10}E_8$*	Water	Silicone oil	Frumkin	> 50	$> 2.5\cdot10^{-2}$	[63]
$C_{12}E_4$	Water	Air	Frumkin	> 30	$\geq 1.1\cdot10^{-2}$	[69]
$C_{12}E_6$	Water	Air	Frumkin	4	$1.4\cdot10^{-4}$	[70]
$C_{12}E_8$	Water	Silicone oil	Frumkin	22.1	$6.86\cdot10^{-6}$	[63]
$C_{12}E_8$	Water	Air	Frumkin	> 17		[64]
$C_{12}E_8$	Water	Air	Frumkin	4–28	$(1–7)\cdot10^{-4}$	[71]
$C_{14}E_8$	Water	Silicone oil	Frumkin	9.40	$2.54\cdot10^{-8}$	[63]
$C_{14}E_8$	Water	Air	Frumkin	> 23		[64]
Triton X-100	53.5% glycerol in water	Silicone oil	Langmuir	9.4	$9.4\cdot10^{-3}$	[58]
Triton X-141	53.5% glycerol in water	Silicone oil	Langmuir	9.3	$8.7\cdot10^{-3}$	[58]
M(D'E_4OH)M**	Water	Air	Frumkin	3	$2.7\cdot10^{-5}$	[72]
M(D'E_8OH)M	Water	Air	Frumkin	5	$1.95\cdot10^{-5}$	[72]
M(D'E_{12}OH)M	Water	Air	Frumkin	10	$2.9\cdot10^{-6}$	[72]

* C_nE_m stays for alkyl polyethylene oxides $CH_3(CH_2)_{n\text{-}1}(OCH_2CH_2)_mOH$.
** M(D'E_nOH)M stays for trisiloxane surfactants with M = $(CH_3)_3SiO$, D′ = $(CH_3)Si(CH_3)_2$, E = OCH_2CH_2, R = -OH, -OCH_3, —H or OAc.

increases with a decrease of drop radius.

It should be stressed that creation of an absolutely new interface is a rare case. In most processes, the creation of a new interface is in reality an expansion of an existing interface which already contains some surfactant. For example, during periodic drop formation, some surfactant remains on the interface after the previous drop detaches, but when the surface expands, new portions of the interface are created during the growth of the next drop. If surfactant replenishment from the bulk is not fast enough, the surface concentration can decrease considerably during expansion and interfacial tension can increase up to that of the clean interface.

3. Drop formation

One of the main advantages of drop microfluidics is the possibility to form a large amount of highly monodisperse drops with high throughput. It is possible also to form several isolated drops to carry out a study at the level of a single drop [73]. The microfluidic drops can be generated in T-junction (Y-junction as a modification), co-flow and flow focusing devices. The gravity force is negligible in microfluidics and therefore the main driving force for drop formation is hydrodynamic interaction between the continuous and dispersed phases, whereas the force opposing interface deformation and drop detachment is interfacial tension.

Co-flow devices usually have cylindrical symmetry and are composed of two co-axial capillaries, one of smaller diameter (normally with a tapered end) for the dispersed phase, sometimes called inner fluid, and one of larger diameter for the continuous phase, sometimes called outer fluid (Fig. 1 a–d). The advantage of co-flow is the small effect of the wetting properties of the channel on drop formation, at least for the drops noticeably smaller than the channel diameter [74]. This comes however with the cost of a more complicated process of device fabrication and the difficulty of building devices with a complicated structure, whereas other geometries can be easily fabricated using soft lithography [75]. The driving forces for interface deformation leading to drop formation in co-flow device are the inertia of the dispersed phase and the shear stress applied from the continuous phase. In the dripping regime (Fig. 1b), drops are formed near the capillary tip, whilst in the jetting regime (Fig. 1c, d) they are formed far downstream. Two different jetting regimes were observed in co-flow devices. Multiple drops can be formed at the end of narrowing jet far downstream of the capillary tip due to Rayleigh-Plateau instability [76] (Fig. 1c). Transition to jetting in this case is caused by an increase of flow rate of continuous phase and corresponding increase of shear stress on the dispersed phase. The relative importance on viscous forces and interfacial tension is characterised by capillary number [77].

$$Ca = \frac{\mu_c u_c}{\gamma} \tag{19}$$

where μ_c is the viscosity of continuous phase, u_c – is the average velocity of continuous phase and γ is the interfacial tension. Another definition of capillary number, often used in drop microfluidics, uses the ratio of elongational or shear stress, $\mu_c G$, to capillary pressure in the drop, γ/L [78].

$$Ca = \frac{\mu_c G L}{\gamma} \tag{19a}$$

Here L is a characteristic length scale, for example drop radius and G is the elongational or shear rate. Transition from dripping to jetting mediated by the continuous phase occurs when the capillary number exceeds a critical value. The polydispersity of drops formed in this jetting regime is higher than in dripping regime.

Another jetting regime (Fig. 1d) was observed in co-flowing device at large values of dispersed phase flow rate and is characterised by widening jet [76]. Transition to this jetting regime depends on Weber number of dispersed phase describing the relative importance of inertia and interfacial tension:

$$We_d = \frac{\rho_d d_d u_d^2}{\gamma} \tag{20}$$

Where ρ_d is the density of dispersed phase, d_d is the diameter of the tip of the dispersed phase channel and u_d is the velocity of dispersed phase. Only one drop at a time is formed in this jetting regime and drops are more monodisperse than in the case of jetting regime driven by continuous phase. It is suggested that drop formation in the jetting regime which is driven by the inertia of the dispersed phase is due to absolute instability of the emerging jet, similar to the dripping regime [79].

The T-junction geometry (Fig. 1 e-h) uses cross-flow of continuous phase to form drops of dispersed phase supplied from the perpendicular channel. Similar to co-flow, drops can be generated in dripping (Fig. 1f) and jetting (Fig. 1 g, h) regime by the shear stress applied by the continuous phase. Jetting regime driven by inertia of the dispersed phase was not observed at the T-junction due to its specific geometry, instead another regime, called squeezing, appears. In this regime (Fig. 1 e), observed at small values of capillary number of continuous phase, the growing drop blocks the cross-section of the output channel. This results in pressure growth behind the drop squeezing it to output channel.

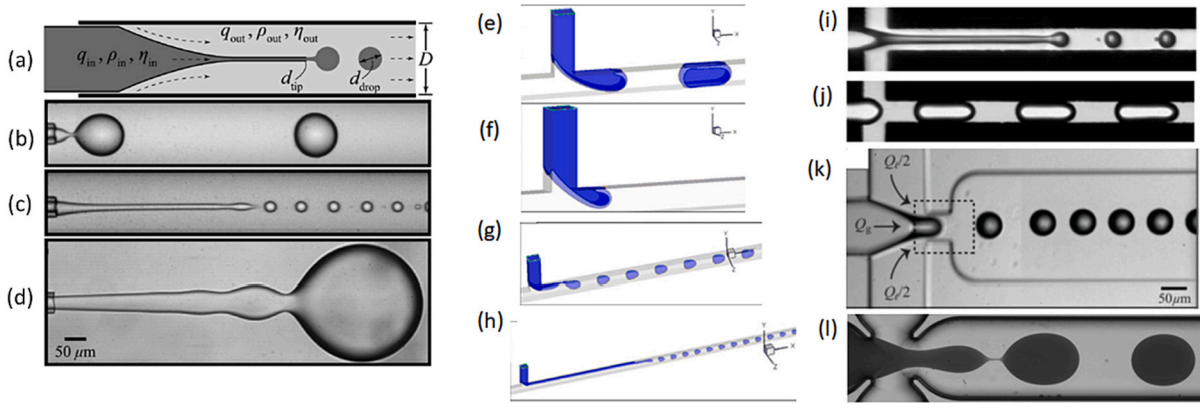

Fig. 1. Microfluidic drop generators; a-d – co-flow: a – device scheme, b – dripping regime, c – jetting regime at large flow rates of continuous phase characterised by a narrowing jet; d – jetting regime at large flow rates of dispersed phase characterised by a widening jet, reprinted with permission from [76]; e-h – cross-flow (T-junction): e – squeezing regime, f – dripping regime, g, h – jetting regime, reprinted with permission from [81]; i-l – flow focusing: i – jetting regime driven by continuous phase, j – squeezing regime, k – dripping regime, l – jetting regime driven by inertia of dispersed phase; i, j - hydrodynamic focusing, k, l – geometrical focusing; i, j reprinted with permission from [82], k – reprinted with permission from [83], l – reprinted with permission from [80].

In flow-focusing devices (Fig. 1 i-l) continuous phase flows symmetrically on both sides of dispersed phase flow, focusing it. Often additional geometrical focusing elements, such as an orifice (Fig. 1 k) or channel constriction (Fig. 1 l) are added to control device performance. In devices with geometric focusing, drop size is determined by the size of the focusing part. In flow focusing devices, all regimes of drop formation found in co-flow and T-junctions have been observed [80].

An additional regime of drop formation, tip-streaming, enabling formation of submicron size droplets in microfluidic devices with a characteristic constriction size of tens of microns was observed in the presence of surfactant and relies completely on surfactant dynamic effects [78,84,85]. This phenomenon resembles the one observed at flow mediated deformation of isolated mm-size drops [77,86,87]. Tip-streaming occurs when the characteristic time of drop deformation is shorter than characteristic time of surfactant exchange between bulk and interface. In such case surfactant is swept to the tip of the formed drop by flow of the continuous phase and is accumulated there due to slow desorption. A large surface concentration corresponds to low values of interfacial tension enabling high curvature at the tip, i.e. formation of the typical conical shape expelling small droplets or a thread breaking up into droplets. Therefore tip-streaming is expected for surfactant with slow equilibration rates, which can be considered close to insoluble on the time scale of drop deformation.

The range of capillary numbers where tip-streaming was observed is $0.4 \leq \mathrm{Ca} \leq 1$ and the viscosity ratio between dispersed and continuous phase $\lambda \leq 0.1$ are similar for microfluidics and mm-sized drops in unconfined flow [78]. In microfluidics, tip-streaming was observed in a certain range of bulk surfactant concentration depending on surfactant used as well as device geometry and properties of continuous and dispersed phase [84]. It reveals itself by the formation of long threads breaking up into small droplets periodically terminated by the formation of large drops. The length of the thread increases with an increase of flow rate ratio between continuous and dispersed phase and surfactant concentration up to $\mathrm{Ca} = 0.5$ [78]. Continuous tip-streaming was achieved in a 3-D microfluidic flow-focusing device [85], where formed emulsions were used for synthesis of submicron particles.

Whatever device is used for drop formation, one of the important parameters controlling the drop size is interfacial tension. Moreover, the regime of drop formation at the same flow rate of continuous and dispersed phase depends on it. The typical time of drop formation in microfluidics is in the range 0.001–1 s, which is comparable with typical characteristic time of adsorption for low molecular mass surfactants [48] and is considerably smaller than adsorption time of polymers and proteins. Therefore, dynamic interfacial tension is a defining factor for drop size and size distribution as well as for regime transitions. Note, although one of the advantages of microfluidics is low material and energy consumption, adjusting the flow rates to produce drops of required size with narrow size distribution and reasonable drop volume fraction in an emulsion is not straightforward and can be time consuming. Understanding and accounting for surfactant dynamic effects will improve considerably the predictability of microfluidic emulsification.

The squeezing and dripping regimes enable formation of the most monodisperse drops, therefore these regimes are preferable for practical applications. Thus, the first problem to be solved is to find the range of flow rates where a given microfluidic device with a given pair of liquids works in the squeezing/dripping regime, i.e. build up a flow map for the device, for example in co-ordinates of the capillary numbers of dispersed and continuous phase [82,88]. If the composition of working liquids changes, the capillary numbers are adjusted to the new parameters. However, if dynamic interfacial tension under the flow conditions in the device is unknown and equilibrium interfacial tension is used instead, then the flow map cannot predict the regime transitions precisely enough.

For example, it was observed in [78] that the critical capillary number at transition from squeezing to dripping to jetting in a flow focusing device increased with an increase of surfactant concentration. Surfactant octaethylene glycol monododecyl ether, $C_{12}E_8$, critical micelle concentration, CMC = 0.1 mM, was dissolved in aqueous dispersed phase and concentration range 0–14.5 CMC was studied. Considering that the capillary number in this study was based on equilibrium interfacial tension, the authors of [78] suggested that this apparent increase in critical capillary number is due to the difference between dynamic interfacial tension at the time scale of interest and equilibrium interfacial tension. The importance of dynamic rather than equilibrium interfacial tension on regime transition was confirmed in [88] where it was shown that dynamic effects are more important for highly active surfactants, with small CMC values having longer equilibration times. It was shown in [89] that the universal flow pattern map in co-ordinates of capillary numbers of continuous and dispersed phase, where regime boundaries are independent of surfactant presence, its type and concentration, can be plotted if capillary numbers are calculated using dynamic instead of equilibrium interfacial tension.

Once the range of flow rates to work in the squeezing/dripping regime is established, it has to be narrowed to produce the drops of required size and volume fraction. Currently, there is no reliable theoretical approach to predict the drop size, however several quite robust semi-empirical equations have been suggested. For drop formation by squeezing in T-junction, the drop size follows the scaling law [90].

$$\frac{L}{W} = 1 + \alpha \frac{Q_d}{Q_c} \tag{21}$$

where L is the drop length, W is the channel width, Q_d and Q_c are the flow rates of dispersed and continuous phase, and α is the geometry dependent coefficient of $O(1)$. The squeezing regime is observed in T-junction devices at $Ca < 10^{-2}$ [90], i.e. its area of existence depends on interfacial tension. Another requirement is the similarity of width of dispersed and continuous phase channels, $W_d/W_c \geq 0.5$ [90]. The length of the drops is always larger than the channel width and is independent of such parameters as the viscosities of continuous and dispersed phases and interfacial tension, because the drop formation is dominated by geometrical restriction of continuous phase flow. A more sophisticated modification of Eq. (21) is derived in [91].

As the capillary number increases, the viscous stress from continuous phase becomes more and more important [92]. The dependence of drop size on capillary number of the continuous phase was observed already at $0.002 < \mathrm{Ca} < 0.01$ in [93], where more general scaling law was suggested

$$\frac{L}{W} = k\left(\frac{Q_d}{Q_c}\right)^{\alpha}\left(\frac{1}{Ca}\right)^{\beta} \tag{22}$$

Applicability of the scaling law Eq. (22) for drop formation at T-junction was confirmed in [94] for 2 surfactant-free cases. After that dynamic interfacial tension was estimated for surfactants dissolved in continuous phase at concentrations above CMC. It was shown in [94] that equilibrium interfacial tension was reached for sodium dodecyl sulphate, the surfactant having the largest CMC value in this study, whereas deviation of DIT from equilibrium value increased with decrease of CMC, surfactant concentration normalised by CMC and time of drop formation.

Eq. (22) was used successfully also for drops formed in a flow-focusing microfluidic device with surfactant dissolved in the dispersed phase [95]. The employed surfactant concentrations were both below and above the CMC. In agreement with [94], it was shown in [95] that for surfactant with highest CMC value and smallest surface activity, dodecyltrimethylammonium bromide, DTAB, dynamic interfacial tension for concentration 0.5 CMC was higher than equilibrium interfacial tension on timescale of drop formation <14 ms, but was close to equilibrium at larger times. DIT was close to equilibrium for concentrations equal to the CMC and above at a time scale ≥5 ms. For a surfactant with larger activity and smaller CMC, SDS, dynamic interfacial tension at a

concentration of 0.7 CMC was noticeably larger than equilibrium value, for concentrations 1 CMC and 1.4 CMC it was only slightly higher than the equilibrium value and equilibrium interfacial tension was reached at higher concentrations. For the most active surfactant studied, Triton X-100, drop size was determined by dynamic surface tension up to concentrations considerably above the CMC. These results are in line with the analysis of characteristic adsorption time given in Section 2. Note, it was suggested in [95] that, for Triton X-100, mixed adsorption kinetics can be expected.

It was found in [95] that an increase in flow rate of the dispersed phase and therefore stronger internal convection resulted in a decrease of DIT, despite a smaller drop formation time for all studied surfactants at concentration where DIT was above equilibrium values. This result agrees with earlier studies [96,97] where drops were formed in co-flow device and in T-junction respectively with surfactant placed in the continuous phase. It confirms the importance of convection during the drop formation for DIT value through decrease of thickness of concentration boundary layer, see Eqs. (11), (12) and (14).

The examples above demonstrate clearly that the surfactant equilibration rate and in particular the dynamic interfacial tension are crucial parameters for prediction of drop size in microfluidics. They also show that microfluidics can be used for measurement liquid/liquid dynamic interfacial tension on short time scale. A detailed discussion of such measurements and their limitation is given in section 6.

4. Drop movement in channels

Once a drop has been formed, it moves through a microfluidic channel network to collection/observation point. Depending on the purpose of drop formation, various processes take place during this movement. If drops are used as templates for solidification, at the collection point they should be stable against coalescence, i.e. surfactant adsorption must be complete. Drops can be particularly prone to coalescence at the exit of a microfluidic device due to the considerable change of flow velocity. A larger intensity of recirculation inside the drop results in faster adsorption. If drops are used as reactors, the reaction has to be completed and thus the mixing inside the drop defined by the flow patterns is of great importance. The flow patterns in straight channels depend on many parameters: channel geometry (cylindrical or rectangular, aspect ratio for rectangular channels), drop size, flow rates, viscosity ratio between continuous and dispersed phase as well as interfacial tension. Note, there is always a considerable difference between the flow patterns in cylindrical and rectangular channels: in rectangular channels the continuous phase can bypass the drop through corners [31,98] changing the flow patterns inside the drop and surfactant distribution over the interface. Flow patterns in surfactant-free microfluidic drops moving in straight channels were thoroughly studied for example in [99–102]. Mixing within the drop intensifies considerably in meandering channels [103,104].

If surfactant has been added to either dispersed or continuous phase, or to both, the flow pattern can be also dependent on adsorption kinetics and surfactant redistribution over the interface due to surface convection. The latter can lead to non-uniform surfactant distribution and surface retardation resulting in retarded recirculation inside the drop. The non-uniform distribution of surfactant can also result from a difference in thickness of adsorption layer as discussed in Section 2. The building of a non-uniform adsorption layer over the interface of a drop moving in a rectangular channel as reported in [5] is shown in Fig. 2 for adsorption of fluorescent surfactant from continuous oil phase. Non-uniformity of the adsorption layer over the surface of a bubble moving in a cylindrical channel [105] and surfactant-laden drop moving in a square channel [51] was found in numerical simulations. It was reported in [105] that the non-uniformity increases with an increase of capillary number, but decreases with an increase of surfactant concentration.

Sweeping of surfactant to the rear of a drop under the high confinement of drop in microfluidic channel can lead to strong

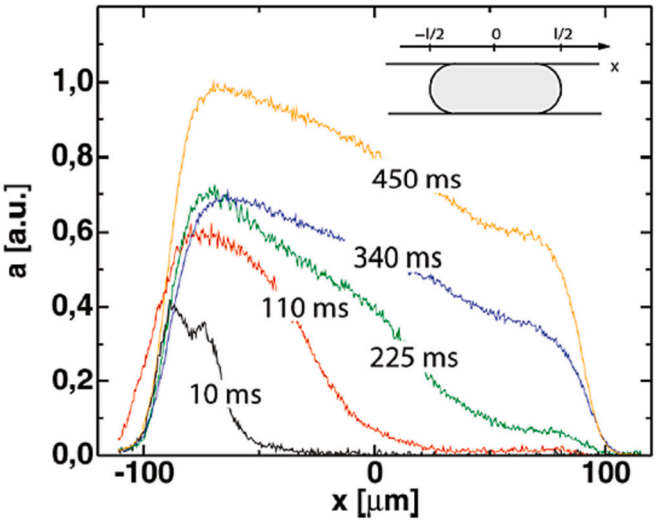

Fig. 2. Distribution of fluorescent surfactant along the drop length as reflected by fluorescence intensity. The label of each curve corresponds to the droplet lifetime after generation. Reprinted with permission from [5].

deformation of the rear part of the drop and finally to tip streaming as shown in Fig. 3a. It should be noted that, during drop formation, surfactant is being swept to the front of the drop, where tip streaming occurs, whereas during drop movement, surfactant is swept to the rear of the drop, where two tails ejecting small droplets are formed near the channel wall [106,107]. Numerical simulations performed for a gas bubble moving in cylindrical channel [108] have shown that the deformation of the rear part can increase drastically resulting in bubble splitting along the channel axis.

Most studies of the effect of surfactant on flow fields in the moving drops were limited to using one surfactant at a single value of concentration and comparing the results with surfactant-free drops. No difference in the flow field between a surfactant-free and surfactant-laden drop moving in rectangular channel was found in [98]. In this study a surfactant, 1.5% of Pico-Surf™ 1, was dissolved in a continuous phase of fluorinated oil HFE7500 (viscosity 1.28 μPa·s) whereas water/glycerol mixture (viscosity 11.5 μPa·s) was used as the dispersed phase. Surprisingly, there was also no difference in drop shape, despite the large, 5 times, difference in interfacial tension, while all other parameters, including drop length and velocity were kept the same.

On the contrary, changes in flow fields within a water drop moving in continuous phase of sunflower oil laden with 1% Span 80 were reported in [109]. It is difficult to reveal the main reason for the difference in the results between [98,109], considering a large number of parameters involved. Despite the same, rectangular, channel size, the channel aspect ratio, W/H, where W is the channel width and H is the channel height, was different: 4:3 in [98] vs 3:2 in [109], as was the viscosity ratio between dispersed and continuous phase, λ, with values of 9 and 0.018 respectively. The molecular mass of Pico-Surf™ 1 is unknown, but considering the nearly 40 times larger viscosity of the continuous phase in [109], it can be assumed that diffusion in this case is slower and therefore surfactant equilibration time is larger. It is interesting to note that a tail-like deformation of the drop rear part was observed in [109] which can be attributed to a considerable excess of interfacial coverage there.

The effect of surfactant dissolved in dispersed phase on flow fields inside the drops moving in rectangular channel with aspect ratio $W/H = 2$ and viscosity ratio $\lambda = 0.125$ was reported in [33]. Four surfactants covering a broad range of surfactant activities (0.01 mM < CMC < 100 mM) and concentrations from 0.1 to 10 CMC have been studied. The flow fields were studied in 5 drop cross-sections uniformly distributed over the drop height. This enabled understanding of the 3D flow

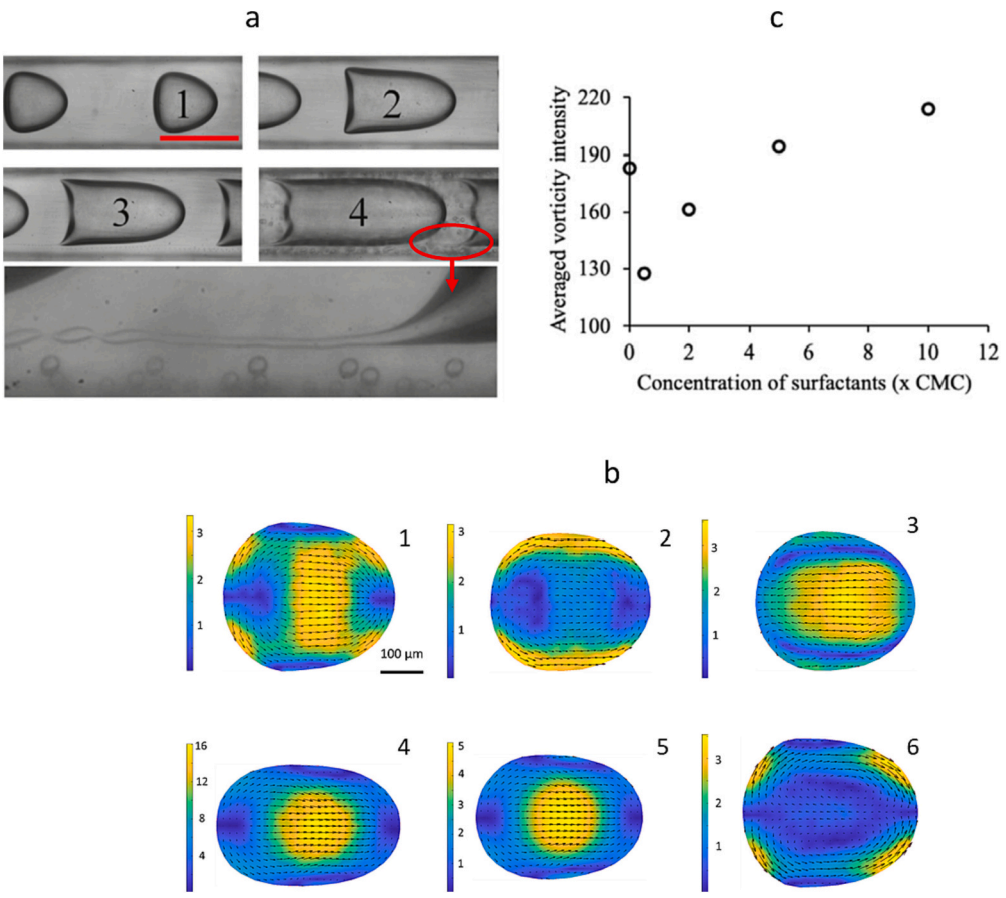

Fig. 3. a: changes in the shape of rear part of a drop moving in a microfluidic channel and formation of satellite droplets due to surfactant redistribution, adapted with permission from [107]; b: flow fields in drops moving in rectangular channel. 1–3 – surfactant-free drop, Ca = 0.013, 1 – middle plane, shows vortices due to interactions with the side walls (top and bottom of the picture), sink at the front and source at the bottom of drop related to vortices due to interactions with top and bottom wall, 2–60 μm from the middle plane, shows vortices related to the corner flow of continuous phase, 3–80 μm from the middle plane, shows the return flow near the top wall, 4 – surfactant-free drop at Ca – 0.04 (middle plane), 5 – surfactant-laden drop, C_{10}TAB c = 135 mM = 1.5 CMC, Ca = 0.037 (middle plane), 6 – surfactant-laden drop, Triton X-100, 0.3 mM = 0.3 CMC, Ca = 0.036 (middle plane), adapted with permission from [33]; c – dependence of vorticity in drop moving through a rectangular channel on surfactant (SDS) concentration, reprinted with permission from [110].

structure. For the surfactant-free drop, flow was formed by 8 main vortices: 4 vortices due to drop interactions with channel walls (Fig. 3 b1 and b3) and 4 vortices related to corner flow of continuous phase (Fig. 3 b2). These vortices were rotating in the opposite direction and the direction and intensity of flow in the middle cross-section of drop was determined by their interaction. Small vortices were also present at the front and rear of the drop due to interaction with continuous phase (Fig. 3 b1).

It was shown in [33] that the effect of surfactant was strongly dependent on surfactant equilibration rate. In the studied range of capillary number, $0.01 < Ca < 0.04$, for quickly equilibrating surfactants (large CMC values) no considerable dynamic effect was observed and flow field structure was completely defined by capillary number (sf Fig. 3 b1, b4 and b5). In this case, surfactant adsorption/desorption was fast enough and interfacial concentration gradients, even if formed, were too small to affect the flow structure. This is in line with the results reported in [111], where no effect of surfactant of the flow fields was found. Surfactant, SDS, was dissolved in continuous phase of water/dimethyl sulfoxide mixture in concentrations of 0.1, 1 and 3 CMC (CMC = 35 mM). The viscosity of continuous phase was 4 mPa·s. Considering the large CMC value and low viscosity of the surfactant-laden phase, the surfactant can be considered as fast equilibrating in [111].

For slowly equilibrating surfactants, adsorption/desorption is slow and therefore surfactant concentration at the rear should be much larger than at the front of the drop. The created gradient of interfacial tension accelerated considerably the corner vortices and suppressed the wall vortices causing flow reversal in the middle plane of the drop [33] (Fig. 3 b6). Note, slowly equilibrating surfactants have high surface activity and are present in solutions at relatively low concentrations. As already mentioned in section 2, in this case adsorption can lead to considerable change in the bulk concentration and the surfactant mass balance should be taken into account. For characteristic sizes of microfluidic drops around 100 μm, surfactant depletion from the bulk can be noticeable at concentrations below 1 mM. For example, Triton X-100 concentration 0.3 mM mentioned in Fig. 3 b6 is the initial bulk concentration, which decreases to around 0.2 mM after the adsorption is completed.

In [110], the effect of surfactant on flow fields in moving drops was carried out by analysing vorticity values in the middle plane of the drop at a constant value of capillary number. For plug (2D confinement) at Ca = 0.001, an addition of fast equilibrating surfactant, SDS, at a concentration below the CMC resulted in lower vorticity near the wall compared to the surfactant-free drop. Increase of SDS concentration above the CMC resulted in an increase of vorticity, which exceeded the one observed in surfactant-free drop at concentrations 5 CMC and above (Fig. 3 c). At larger Ca = 0.005 similar qualitive behaviour was observed, but despite an increase with concentration, vorticity remained below that for surfactant-free case at concentrations up to 10 CMC, due to the manifestation of larger Marangoni stresses at larger drop velocity.

The results of [110] agree with those presented in [33] for similar surfactant DTAB, with 2 times higher CMC value. According to [33], the difference between minimum and maximum velocity in the middle plane decreased with an increase of surfactant concentration at concentrations below the CMC and increased considerably at concentration around 2 CMC. Smaller differences between maximum and minimum velocity in surfactant laden drops is also seen in Fig. 3 b4 and b5. It should be however noted that besides Marangoni stresses there is another contribution to smaller vorticity inside the drop. To keep capillary number constant, a surfactant-laden drop should have smaller velocity and therefore smaller shear stress near the wall. The effect of wall shear stress was demonstrated in [110] by comparing vortices within a plug with those within a pancake shaped drop circular in the plane of observation (i.e. drop size smaller than the channel width)

while keeping the same Ca = 0.001. In this case, vorticity within the pancake drop was considerably smaller than for the plug due to weaker interaction with wall and only mildly dependent on the surfactant concentration. When SDS in [110] was replaced by a slowly equilibrating surfactant (Tween 20), recirculation within the drop was considerably slower in all surfactant-laden drops, up to concentration of 10 CMC, but also slower than in SDS-laden drops indicating considerably larger Marangoni stresses.

Thus, the presence of surfactant changes the flow characteristics for drop moving in microfluidic channels even at small capillary numbers Ca ~ 0.001. The effect is more pronounced for surfactants with higher activities (smaller CMC values) for which even flow inversion within a drop can be observed. Accumulation of surfactant at the rear of the drop can result in tip-streaming.

5. Drop coalescence

Drop coalescence is another major microfluidic operation. Besides the study of coalescence itself, for example for better understanding foam and emulsion stability, it enables triggering a chemical reaction by bringing reagents together. In many cases this is the only feasible path for microfluidic analysis/synthesis, in particular if reaction is very fast and products can clog the channel. Drop coalescence in microfluidics can be induced using active methods, such as an imposed electrical field [112] and passive methods, based on device geometry. Passive methods include various coalescence chambers enabling study of an ensemble of drops under a mild flow [2,7] or study of the interaction between pairs of drops under various well-controlled flow conditions [113–115], for example providing compression/extension flow patterns similar to a Taylor four-roll mill flow [8,86].

Surfactants sterically stabilise drops against coalescence. Ionic surfactants provide additional contribution to electrostatic stabilisation, although this effect can be reversed if the surfactant charge is opposite to the charge of the surfactant-free surface. However even in this case, at large surfactant concentrations, surface recharges and the absolute value of the final zeta potential can be considerably larger than that for the bare surface. Surfactant dynamic effects are important for drop stability against coalescence, in particular, by slowing down film drainage. When a continuous phase liquid flows out of film separating two drops, it moves surfactant at the interface in a direction from the centre of film to the periphery. If bulk surfactant in the film is unable to restore a uniform interfacial concentration, the surfactant concentration gradients result in Marangoni stresses retarding outflow of liquid from the film. Microfluidic studies on coalescence of individual drops allow this effect to be observed albeit indirectly. Emulsion stability was measured in [1] by calculating the changes in the average drop volume when the emulsion was moving along the microfluidic channel for residence time up to 7.36 s. Improvement in the emulsion stability on that time scale was observed at a concentration of surfactant, SDS, $2\bullet10^{-4}$ mM, >3 orders of magnitude below CMC value. Analysis performed by the authors of [1] has demonstrated that the only reason for such stabilisation can be Marangoni stresses.

In [113], the dependence of the time span between contact of two drops and their coalescence (film drainage time) was studied as a function of numerous process parameters including concentration of surfactant, Span 80, in the continuous oil phase. It was found, that in surfactant-free case and at small surfactant concentrations, film drainage time normalised by drop size and approach velocity increases with an increase of continuous phase viscosity, however it becomes independent of viscosity at larger surfactant concentrations, up to 2 CMC. It was suggested in [113] that at larger concentrations, the effect of Marangoni stresses on film drainage becomes dominant and overcomes considerably the effect of continuous phase viscosity.

The presence of surfactant in one or both coalescing drops can considerably affect the coalescence kinetics as well as mixing during and after coalescence. If one drop has smaller interfacial tension due to a presence of surfactant, immediately after contact it starts to envelop the other drop due to interfacial tension gradient. The prolongation of this Marangoni flow should depend on surfactant concentration and relation between timescale of surfactant equilibration and timescale of Marangoni flow, Eq. (9). If there is enough of quickly equilibrated surfactant, it will be replenished at the interface of the initially surfactant-laden drop, while it will be dissolved into the bulk phase of initially surfactant-free drop. In this case the interfacial tension gradient and Marangoni flow can persist for relatively long time, weakening as the surfactant concentration in the two drops equilibrates. However, if the concentration of surfactant is small and/or equilibration rate is slow, the concentration gradient will be reduced quickly and the Marangoni flow fades out. Another effect related to the difference in interfacial tension between the coalescing drops is the difference in capillary pressure. For drops of the same size, the capillary pressure is larger in surfactant-free drop and it will squeeze it inside the surfactant-laden drop. The persistence of this effect is also determined by surfactant concentration and equilibration rate.

The coalescence of two miscible drops of pure liquids having different interfacial tension with continuous phase was addressed numerically for stationary drops in an unbounded geometry and drops flowing in cylindrical tube [38]. The resulting mixing at coalescence of stationary drops is shown in Fig. 4a. For drops moving in a cylindrical tube the mixing intensity depends on interactions of the flow fields generated by drop motion in the tube and flow fields due to Marangoni stresses, i.e. it depends on the order of drops along the channel [38].

An experimental study on the coalescence of surfactant-laden and surfactant-free drops in rectangular microfluidic channel [6] confirmed the prediction of numerical simulations [38]. If the surfactant-laden drop is first in the flow direction, i.e. the direction of viscous shear stresses near the walls coincide with direction of Marangoni stresses, the penetration of surfactant-free drop inside the surfactant-laden drop on the short time scale and mixing on the longer time scale are both faster (Fig. 4b).

6. Measurement of dynamic interfacial tension

As shown in the previous sections, the dynamic effects of surfactant are of great importance for all basic microfluidic operations: drop formation, transfer/sorting and coalescence. They are also crucial for many industrial multiphase flows. For example the drop size in various industrially relevant emulsification processes is defined by interfacial tension on the time scale of drop formation, which ranges from 0.1 ms to tens of milliseconds [116]. The stability of formed drops against coalescence is directly related to the completeness of the stabilising surfactant layer on the same time scale. Therefore, the measurement of liquid/liquid dynamic interfacial tension on the millisecond time scale is of great importance and microfluidics can provide multiple approaches to such measurements. Below these approaches, their advantages and limitations are discussed.

The most frequently used microfluidic method for measurement of dynamic interfacial tension enabling data acquisition at millisecond and even sub-millisecond time scale is based on drop size, for example by using Eq. (22) [94,95] or other available empirical correlations between the drop size and interfacial tension [52,82,117]. Considerable improvement in the prediction of drop size can be achieved by using data driven models [118]. Drop formation time can be used as well, considering that the drop volume is equal to its product with the flow rate of dispersed phase. First the pair of liquids of interest, continuous and dispersed phase, is studied over a broad range of flow rates, i.e. drop formation times. Drops are formed without surfactant and with surfactant(s) of high concentration or for example water/alcohol mixtures, assuring that the equilibrium interfacial tension was reached on the timescale of drop formation. Obtained drop sizes are then used to fit into correlation equation and find its parameters. Knowing these parameters, dynamic interfacial tension for the required surfactant concentration

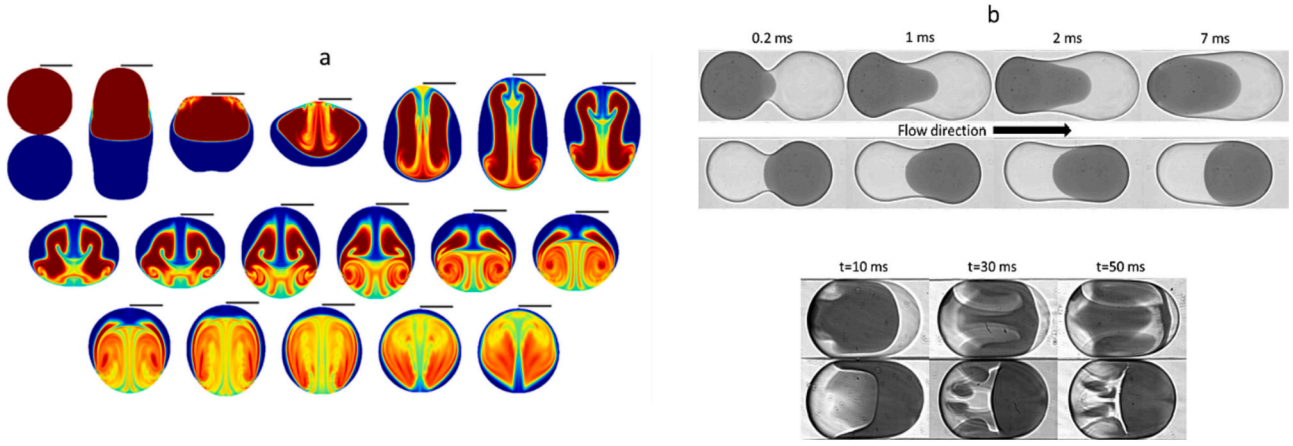

Fig. 4. a: results of numerical simulations on coalescence of two motionless drops in unbounded liquid. The top drop has higher interfacial tension, the relative difference in interfacial tension between drops $(\gamma_1 - \gamma_2)/\gamma_1 = 0.4$. The black lines are equal to the initial drop radius. Reprinted with permission from [38]. Experimental data on coalescence and following mixing of surfactant-laden (light) and surfactant-free (dark) drop in microfluidic channel. Reprinted with permission from [6].

and time can be found, provided that the values of experimental parameters are within the range used for fitting. The essential requirement of this method is the same regime of drop formation and the same drop shape (spherical drop, pancake or plug) for DIT measurement and calibration. The fitted parameters of the correlation change with drop shape [52], because a spherical drop can grow in all three dimensions, a pancake can grow in 2-D and plug size changes only in 1-D, along the channel axis.

Direct evaluation of interfacial tension from the force balance on the drops formed in dripping regime was also used, in particular for drops formed in co-flow device with cylindrical symmetry [74]. It was assumed in [74] that the inertia and momentum force as well as effect of gravity can be neglected. In this case drop detachment is determined by the balance of interfacial tension and viscous drag. The viscous drag force depends on the relative velocity of the drop and continuous phase, choice of which is rather tricky. In [74], the drag force was calculated as

$$F_D = k(u_c - u_d)d_d\mu_c \tag{23}$$

where k is the geometry dependent coefficient, d_d is the drop diameter and u_c, u_d are average velocities of continuous and dispersed phase respectively calculated as

$$u_c = \frac{4Q_c}{\pi\left(D_{in}^2 - d_d^2\right)} \tag{24}$$

$$u_d = \frac{4Q_d}{\pi d_d^2} \tag{25}$$

where D_{in} is the inner diameter of continuous phase capillary.

Interfacial tension force was calculated in [74] as

$$F_{IT} = \frac{\pi d_n^2 \gamma}{d_d} \tag{26}$$

where d_n is the diameter of dispersed phase channel. Equations for F_d and F_{IT} provides an expression for DIT at the time of drop formation depending on normalised drop size d_d/d_n.

Uncertainties related to using average velocities in the equation for the drag force can be partially accounted for by the calibration process used to fit k. The calibration was made using 1 pair of liquids and then IT was measured for four other pairs of liquids including pure liquids and surfactant solutions of high concentrations. The measured IT was an equilibrium value and a good agreement was found with values measured by traditional macroscopic methods. Therefore, this method seems quite reliable for measurement of equilibrium IT. Although the authors of [74] stress that there can be problems with measurement of DIT because k can be affected by non-uniform surfactant distribution and Marangoni stresses, they still used the approach to measure DIT of SDS and CTAB [96]. To minimize the effect of non-uniform surfactant distribution, only concentrations above CMC have been used.

The problem of possible change of calibration parameters found for pure liquids/concentrated surfactant solutions is important also when using various empirical formulas. In general, the main problem to be solved to increase the reliability and usefulness of the approach based on the drop size is the applicability of obtained results for drop formation in devices of various architecture and in unbounded liquid. The essential point is that surfactant adsorption is carried out on the surface of growing drop. During calibration with surfactant-free liquid or with concentrated surfactant solution interfacial tension is constant over the whole process of drop growth. The situation is completely different for surfactant solution where a DIT effect is expected. Firstly, after detachment of previous drop, the retracted liquid interface is not free of surfactant, but has some surface coverage depending on previous history, i.e. at the beginning of drop formation DIT is not equal to interfacial tension of solvent, but is noticeably lower. When the surface begins to deform due to influx of dispersed phase, the surface area, A, increases and the relative rate of the surface growth is the fastest at the beginning and slows down with time. It is easy to calculate that for spherical drop it is inversely proportional to time [119].

$$\frac{1}{A}\frac{dA}{dt} = \frac{2}{3t} \tag{27}$$

Therefore, at the beginning of the drop growth, DIT remains constant or even increases with time before it starts to decrease, depending on surfactant supply rate [120]. Moreover, the radius of curvature changes continuously during the drop growth and the thickness of the adsorption depletion layer changes as well, see Eqs. (6), (7). This means that the rate of diffusion limited adsorption is not constant, but varies with time. Thus, the DIT measured by drop size in microfluidic device is not the same as, for example, DIT corresponding to the adsorption of the surfactant at the clean surface of the drop of constant size and cannot be transferred directly to other processes, including drop formation under different conditions.

From the results available so far, it appears that the measured DIT depends on device architecture and the models used. In particular, according to [96] (co-flow, drop size 30–120 μm, model based on Eqs. (23)–(26)) considerable deviations from equilibrium IT (> 20%) on timescale 5–15 ms were observed even at concentration SDS of 16 CMC, whereas DST deviated <20% from equilibrium value already at

concentration of 2 CMC in [95] (flow focusing, drop size 80–140 μm, model based on Eq. (22)). The difference is rather surprising because in [96] surfactant was dissolved in continuous phase, whereas in [95] it was dissolved in dispersed phase, so the thickness of adsorption layer should be smaller in the former case, sf Eqs. (6) and (7). Moreover, in [95] surfactant was dissolved in glycerol/water mixture with viscosity 7 times larger than viscosity of water used in [96] and therefore 7 times smaller diffusion coefficient. The reason for the difference in the results can be the dependence of flow fields and therefore the thickness of concentration boundary layer on device geometry and variability of the effect of non-uniform surfactant distribution over the surface of the growing drop. At the same time there is a good agreement for SDS concentrations ≥2 CMC between [94,95] (T-junction, drop size 228–426 μm, surfactant dissolved in continuous phase of water) where the same model of Eq. (22) was used. Obviously, more thorough studies are required to make reliable conclusions about reliability and general applicability criteria of this method of DIT measurement.

Another question is to which extent the viscosity ratio of continuous to dispersed phase affects the drop size. If this ratio changes due to change of continuous phase viscosity then the effect is completely accounted for by changes in capillary number [52,94]. It is however not clear whether and to which extent the parameters of Eq. (22) and other empirical correlations are sensitive to changes in viscosity of dispersed phase.

Considering the short time scale of DIT measurements, the mutual solubility of dispersed and continuous phase can be of importance. Long time scale measurements are usually performed under conditions of quasi-equilibrium between these close to the interface, whereas on short time scale, surfactant adsorption can be accompanied by mutual saturation fluxes between continuous and dispersed phase affecting local surfactant solubility and adsorption properties. It would be of interest to compare the short time scale DIT for the cases of mutually saturated and unsaturated phases, especially those of industrial importance. It is noticeable, that in some cases, the mass transfer between the continuous and dispersed phases results in the development of convective instabilities providing additional acceleration of mass transfer, see for example [121] and references herein.

In several studies, dynamic interfacial tension was calculated from simultaneous (synchronised) measurement of capillary pressure and the main curvature of the growing drop [122–124]. Capillary pressure, Pc, under curved interface depends only on the shape of the interface and interfacial tension as (Young-Laplace equation)

$$P_c = \gamma\left(\frac{1}{R_1}+\frac{1}{R_2}\right) \tag{28}$$

where R_1 and R_2 are the principal radii of curvature.

This method is a microfluidic extension of the well-known growing drop/bubble method [125–127] for which commercial equipment is available. The latter uses a spherical bubble/drop formed at the tip of capillary of radius 0.1–0.5 mm and attains timescale down to milliseconds for liquid/air interface [127] and 100 ms for liquid/liquid interface [126]. The advantage of using capillary pressure is the possibility to monitor interfacial tension not just at the moment of drop detachment, but continuously during the drop growing cycle. Obviously, the limitations of the drop size method, such as uncertainty in the initial surfactant concentration after the detachment of the previous drop and surfactant redistribution over the drop surface apply also for this method.

So far, the microfluidic measurement of dynamic interfacial tension based on capillary pressure was carried out in two configurations: co-flow and cross-flow (T-junction). Co-flowing device was employed to

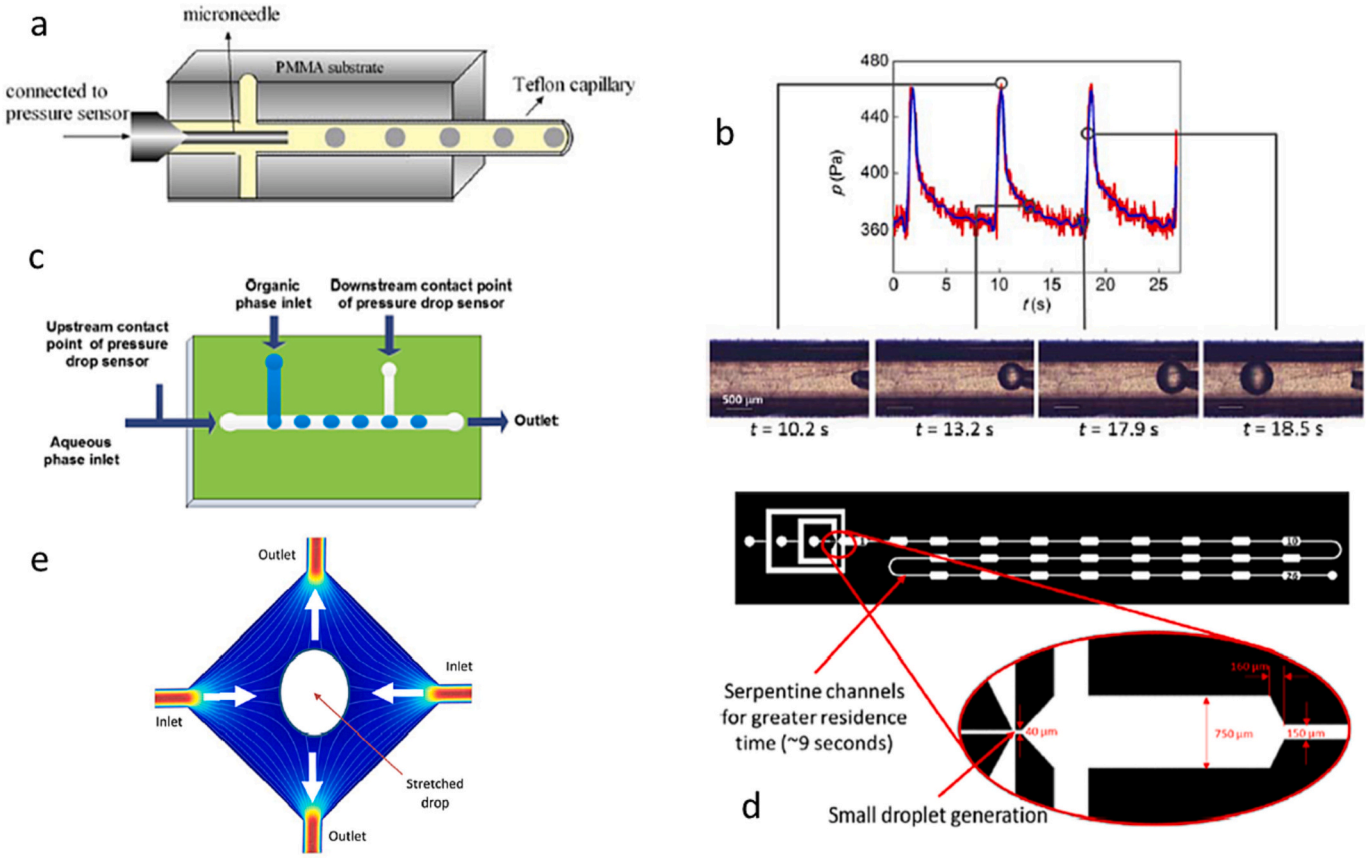

Fig. 5. Methods of measurement of dynamic interfacial tension: a, b – capillary pressure co-flow, reprinted with permission from [123]; c – capillary pressure T-junction, reprinted with permission from [122]; d – drop deformation in contractions/expansions, reprinted with permission fron [130]; e – drop deformation in contraction/extension flow, reprinted with permission from [129].

measure mass transfer of surface-active solutes between dispersed and continuous phase [123,124], with both transfer directions considered. Pressure was measured in the dispersed phase channel as shown in Fig. 5a. It oscillated with period equal to the drop formation time due to change of capillary pressure related to the change of interfacial tension and/or curvature radius of the drop as shown in Fig. 5b. The pressure increased fast in the initial stage of drop formation and reached a maximum approximately at the time when drop radius was equal to the capillary radius. For pure liquid, the maximum capillary pressure corresponds exactly to the minimum radius of drop, but for surfactant solutions there can be a shift related to the changing interfacial tension. Capillary pressure decreases gradually with further increase of the drop size, Fig. 5b.

It is well known from the theory of growing drop that besides the capillary pressure, dynamic effects related to the liquid flow contribute to measured pressure value [125,127]. It was assumed in [123,124] that the hydrodynamic pressure contribution is constant during the cycle of drop formation in microfluidic device and is independent of the presence of surfactant. This constant part was derived from the calibration measurements based on surfactant-free liquid and was later used for calculation of interfacial tension of surfactant-laden liquid. The assumption above is rather rough because the interfacial velocity as well as velocity distribution in continuous phase always depend on the size of the growing drop. Nevertheless, this approximation looks quite acceptable at least for frequencies of drop formation below 1.5 Hz because the interfacial tension calculated for surfactant-free system was very close to that measured by the pendant drop technique. At larger frequencies of drop formation, the calculated value of interfacial tension for surfactant-free system decreases more and more in comparison to the real value [123,124]. As a result, the time to assess the interfacial tension with this method hardly goes below 0.1 s, which is similar to the time accessed with the macroscopic growing drop method. The authors ascribe this time limitation to the sensor effects. The interfacial tension of surfactant solutions at small frequencies was then calculated as

$$\gamma = \frac{R(\mathrm{P} - P_d)}{2} \tag{29}$$

where P is the measured instantaneous value of pressure, $\mathrm{P_d}$ is the pressure loss due to dynamic effects of liquid flow, and R is the drop radius of curvature at the apex. The authors of [123,124] have chosen the point at the apex as characteristic of measuring of capillary pressure arguing that drop curvature in this point is least of all affected by the flow of continuous phase. Note, the advantage of co-flowing device is its axial symmetry, making two principal curvature radii at apex equal to each other and easily measurable from the high-speed recording of the growing drop.

Pressure drop over the part of main channel including T-junction (Fig. 5c) was used for measurement of interfacial tension in [122]. The shape of drop formed in T-junction is more complicated and less symmetrical compared to co-flow. Therefore, the relation between the drop shape and capillary pressure is not straightforward. The authors of [122] used an approach suggested in [91], where the pressure difference over the growing in T-junction drop is equal to difference in capillary pressure between the front and rear part of the drop

$$\Delta P = \gamma\left(\frac{1}{R_{1f}} + \frac{1}{R_{2f}} - \frac{1}{R_{1r}} - \frac{1}{R_{2r}}\right) \tag{30}$$

The curvature radii in the plane of observation for the front R_{1f} and rear, R_{1r} of the drop are easily extracted from the drop image, whereas it is assumed that the radius of curvature perpendicular to the plane of observation is always equal to half of channel height at the front of the drop, $R_{2f} = H/2$, and is equal to min (H/2; r) at the rear of the drop, where r is radius of the drop neck. This assumption contributes to the error of the method. Eq. (30) is applicable only if the pressure inside the drop is constant, what is not exactly true in the case of a growing drop. This is another contribution to the error of this method. Measurements performed in [122] for pure liquid show that the maximum measured pressure difference gradually increases with an increase of flow rate, but in the studied flow rate range the difference was within 10%. It can therefore be concluded that the dynamic interfacial tension can be measured using capillary pressure method in T-junction device at least at small capillary numbers, Ca $<$ 0.01, but calibration measurements with pure liquid are required to validate results.

Dynamic interfacial tension can also be measured using drop deformation in constrictions embedded in microfluidic device (Fig. 5d) or in compression/extension flow (Fig. 5e). The equation used for calculations is, for example, dependence of drop deformation on capillary number [128,129]. Using multiple contractions and expansions dependence of dynamic interfacial tension on time can be extracted [130].

Taking into account that after the drop is formed it has to move for some time in a straight channel before the first constriction, the accessible time of measurement with this method is of the order of seconds, i.e. similar to traditional macroscopic techniques, such as drop profile tensiometry. The advantages of the microfluidic method are the possibility of measurement of DIT on small drops relevant for many industrial applications, where the mass transfer can be different due to drop curvature, see Eqs. (6) and (7). Considering convection in both dispersed and continuous phase, combined kinetics + diffusion limited adsorption mechanism can be achieved [64] giving way to measurement of adsorption and desorption coefficients (see Eq. (15) and discussion around it). Microfluidic tensiometry based on multiple sequential drop deformation can be also very useful for measuring dynamic interfacial tension of slowly equilibrating solutes, such as proteins. The characteristic adsorption time in this case can be quite long, but the applicability of macroscopic techniques is limited due to the large cost and small availability of samples whereas microfluidic technique enables measurement using nanolitre size droplets.

7. Conclusions and proposals for future work

Dynamic effects due to surfactant presence in continuous or/and dispersed phase are important through all stages of drop processing in a microfluidic device. Regime of drop formation and drop size depend on dynamic interfacial tension which, in turn, can be affected by non-uniform surfactant distribution over the growing drop surface. In particular, non-uniform surfactant distribution can result in tip-streaming from the front of forming drop or from the rear of the drop moving in a microfluidic channel. Kinetics of drop coalescence and mixing within the drop after coalescence are also affected by surfactant presence and distribution, especially if the coalescing drops have different interfacial tension. The flow patterns and mixing within a drop moving in microfluidic channel are dependent on the added surfactant. Effect of dynamic interfacial tension on drop formation, deformation in flow fields and coalescence derived from microfluidic experiments provides valuable information for choice of surfactant type and concentration in industrial emulsion and foam formulations.

Dynamic surfactant effects strongly depend on surfactant properties, in particular on relative values of characteristic time scale of surfactant adsorption/desorption and surface deformation. If the surfactant equilibrates very fast, then the surfactant solution behaves as a pure liquid with interfacial tension equal to the equilibrium value. If the interface deforms much faster than surfactant equilibrates, the surfactant can be considered as insoluble. For diffusion-controlled surfactant dynamics, the characteristic adsorption time increases with an increase of surfactant activity ($\sim b^2$) or with decrease of CMC value ($\sim CMC^{-2}$). It is however difficult to estimate relevant time scales precisely, because they depend on many factors including interdependent flow patterns in both continuous and dispersed phase and surfactant distribution. Better understanding of surfactant dynamics in microfluidic multiphase flows can be achieved by using data driven models and computational fluid dynamics (CFD) simulations. Both approaches require, however, well-

tailored experiments for the model development and validation. CFD additionally requires reliable values of physical parameters used, such as type and parameters of adsorption isotherms, adsorption and desorption coefficients, models for and characteristic times of micelle disintegration and diffusion coefficients. The progress in predictability of processes in microfluidic drop devices will be determined to the large extent by the availability experimental data of high fidelity.

Considering the short time scales involved, microfluidic approaches for the measurement of dynamic interfacial tension are quickly developing during the last decade. They include methods based on drop deformation, simultaneous measurement of capillary pressure and drop shape, or drop size. The last method enables measurement of DIT on millisecond and even sub-millisecond time scale not accessible by traditional macroscopic methods for liquid/liquid interfaces. Another advantage of microfluidic methods is the possibility to use small sample volume, which is important while working with very expensive or rare samples. Broad application of microfluidic methods of DIT measurement requires better understanding of related processes to estimate the uncertainty of measured values and their general relevance. How can the DIT at the given time measured in one microfluidic device be used for different microfluidic devices? How does it change if device is scaled up/down or some of dimensions are changed? How can it be extrapolated to industrially relevant processes of emulsification? To answer these questions considerable efforts in theoretical treatment of the problem requiring both numerical simulations and experiments are necessary.

Declaration of Competing Interest

The authors declare that they have no known competing financial interests or personal relationships that could have appeared to influence the work reported in this paper.

Data availability

No data was used for the research described in the article.

Acknowledgements

This work was funded by the Engineering and Physical Sciences Research Council, UK, through the PREMIERE Programme Grant EP/T000414/1.

References

[1] Krebs T, Schroën K, Boom R. Coalescence dynamics of surfactant-stabilized emulsions studied with microfluidics. Soft Matter 2012;8.
[2] Krebs T, Schroen K, Boom R. A microfluidic method to study demulsification kinetics. Lab Chip 2012;12:1060–70.
[3] Muijlwijk K, Colijn I, Harsono H, Krebs T, Berton-Carabin C, Schroën K. Coalescence of protein-stabilised emulsions studied with microfluidics. Food Hydrocoll 2017;70:96–104.
[4] Hinderink EBA, de Ruiter J, de Leeuw J, Schroën K, Sagis LMC, Berton-Carabin CC. Early film formation in protein-stabilised emulsions: insights from a microfluidic approach. Food Hydrocoll 2021:118.
[5] Baret JC, Kleinschmidt F, El Harrak A, Griffiths AD. Kinetic aspects of emulsion stabilization by surfactants: a microfluidic analysis. Langmuir. 2009;25:6088–93.
[6] Kovalchuk NM, Reichow M, Frommweiler T, Vigolo D, Simmons MJH. Mass transfer accompanying coalescence of surfactant-laden and surfactant-free drop in a microfluidic channel. Langmuir. 2019;35:9184–93.
[7] Dudek M, Fernandes D, Helno Herø E, Øye G. Microfluidic method for determining drop-drop coalescence and contact times in flow. Colloids Surf A Physicochem Eng Asp 2020:586.
[8] Yi H, Fu T, Zhu C, Ma Y. Local deformation and coalescence between two equal-sized droplets in a cross-focused microchannel. Chem Eng J 2022;430.
[9] Del Giudice F, D'Avino G, Maffettone PL. Microfluidic formation of crystal-like structures. Lab Chip 2021;21:2069–94.
[10] Ho TM, Razzaghi A, Ramachandran A, Mikkonen KS. Emulsion characterization via microfluidic devices: a review on interfacial tension and stability to coalescence. Adv Colloid Interface Sci 2022;299:102541.
[11] Schroen K, Berton-Carabin C, Renard D, Marquis M, Boire A, Cochereau R, et al. Droplet microfluidics for food and nutrition applications. Micromachines (Basel) 2021:12.
[12] Stucki A, Vallapurackal J, Ward TR, Dittrich PS. Droplet microfluidics and directed evolution of enzymes: an intertwined journey. Angew Chem Int Ed Engl 2021;60:24368–87.
[13] Shi H, Nie K, Dong B, Long M, Xu H, Liu Z. Recent progress of microfluidic reactors for biomedical applications. Chem Eng J 2019;361:635–50.
[14] Clausell-Tormos J, Lieber D, Baret JC, El-Harrak A, Miller OJ, Frenz L, et al. Droplet-based microfluidic platforms for the encapsulation and screening of mammalian cells and multicellular organisms. Chem Biol 2008;15:427–37.
[15] Luo T, Fan L, Zhu R, Sun D. Microfluidic single-cell manipulation and analysis: methods and applications. Micromachines (Basel) 2019:10.
[16] Sarkar S, Sabhachandani P, Stroopinsky D, Palmer K, Cohen N, Rosenblatt J, et al. Dynamic analysis of immune and cancer cell interactions at single cell level in microfluidic droplets. Biomicrofluidics. 2016;10:054115.
[17] Antona S, Platzman I, Spatz JP. Droplet-based cytotoxicity assay: implementation of time-efficient screening of antitumor activity of natural killer cells. ACS Omega 2020;5:24674–83.
[18] Sarkar S, Cohen N, Sabhachandani P, Konry T. Phenotypic drug profiling in droplet microfluidics for better targeting of drug-resistant tumors. Lab Chip 2015;15:4441–50.
[19] Mohamed MGA, Ambhorkar P, Samanipour R, Yang A, Ghafoor A, Kim K. Microfluidics-based fabrication of cell-laden microgels. Biomicrofluidics 2020;14:021501.
[20] Maeki M. Microfluidics for pharmaceutical applications. In: Santos HA, Liu D, Zhang H, editors. Microfluidics for pharmaceutical applications. Elsevier; 2019. p. 101–19.
[21] Kashani SY, Afzalian A, Shirinichi F, Moraveji MK. Microfluidics for core-shell drug carrier particles - a review. RSC Adv 2020;11:229–49.
[22] Hirama H, Ishikura Y, Kano S, Hayase M, Mekaru H. Monodispersed sodium hyaluronate microcapsules for transdermal drug delivery systems. Mater Adv 2021;2:7007–16.
[23] Elvira KS, Casadevall i Solvas X, Wootton RC, de Mello AJ. The past, present and potential for microfluidic reactor technology in chemical synthesis. Nat Chem 2013;5:905–15.
[24] Arai K, Osaka Y, Haneda M, Sato Y. Cyclic telluride reagents with remarkable glutathione peroxidase-like activity for purification-free synthesis of highly pure organodisulfides. Cat Sci Technol 2019;9:3647–55.
[25] Galvan-Chacon VP, Costa L, Barata D, Habibovic P. Droplet microfluidics as a tool for production of bioactive calcium phosphate microparticles with controllable physicochemical properties. Acta Biomater 2021;128:486–501.
[26] Chen M, Bolognesi G, Vladisavljevic GT. Crosslinking strategies for the microfluidic production of microgels. Molecules. 2021;26.
[27] Moreira A, Carneiro J, Campos JBLM, Miranda JM. Production of hydrogel microparticles in microfluidic devices: a review. Microfluidics Nanofluidics 2021;25.
[28] Solsona M, Vollenbroek JC, Tregouet CBM, Nieuwelink AE, Olthuis W, van den Berg A, et al. Microfluidics and catalyst particles. Lab Chip 2019;19:3575–601.
[29] Kubendhiran S, Bao Z, Dave K, Liu R-S. Microfluidic synthesis of semiconducting colloidal quantum dots and their applications. ACS Appl Nano Mater 2019;2:1773–90.
[30] Nathanael K, Pico P, Kovalchuk NM, Lavino AD, Simmons MJH, Matar OK. Computational modelling and microfluidics as emerging approaches to synthesis of silver nanoparticles – a review. Chem Eng J 2022;436.
[31] Fuerstman MJ, Lai A, Thurlow ME, Shevkoplyas SS, Stone HA, Whitesides GM. The pressure drop along rectangular microchannels containing bubbles. Lab Chip 2007;7:1479–89.
[32] Ma S, Huck WT, Balabani S. Deformation of double emulsions under conditions of flow cytometry hydrodynamic focusing. Lab Chip 2015;15:4291–301.
[33] Kovalchuk NM, Simmons MJH. Effect of surfactant dynamics on flow patterns inside drops moving in rectangular microfluidic channels. Colloids Interfaces 2021:5.
[34] Douville NJ, Zamankhan P, Tung YC, Li R, Vaughan BL, Tai CF, et al. Combination of fluid and solid mechanical stresses contribute to cell death and detachment in a microfluidic alveolar model. Lab Chip 2011;11:609–19.
[35] Gregoriades N, Clay J, Ma N, Koelling K, Chalmers JJ. Cell damage of microcarrier cultures as a function of local energy dissipation created by a rapid extensional flow. Biotechnol Bioeng 2000;69:171–82.
[36] Blanchette F, Messio L, Bush JWM. The influence of surface tension gradients on drop coalescence. Phys Fluids 2009;21.
[37] Kovalchuk NM, Chowdhury J, Schofield Z, Vigolo D, Simmons MJH. Study of drop coalescence and mixing in microchannel using ghost particle velocimetry. Chem Eng Res Design 2018;132:881–9.
[38] Blanchette F. Simulation of mixing within drops due to surface tension variations. Phys Rev Lett 2010;105:074501.
[39] Ward AFH, Tordai L. Time-dependence of boundary tensions of solutions I. the role of diffusion in time-effects. J Chem Phys 1946;14:453–61.
[40] Lin SY, McKeigue K, Maldarelli C. Diffusion-controlled surfactant adsorption studied by pendant drop digitization. AIChE J 1990;36:1785–95.
[41] Makievski AV, Loglio G, Kragel J, Miller R, Fainerman VB, Neumann AW. Adsorption of protein layers at the water/air interface as studied by axisymmetric drop and bubble shape analysis. J Phys Chem 1999;103:9557–61.
[42] Surfactants: Chemistry, interfacial properties, applications. Amsterdam, The Netherlands: Elsevier; 2001.
[43] Joos P. Dynamic surface phenomena. Utrecht, The Netherlands: VSP; 1999.
[44] Miller R, Aksenenko EV, Fainerman VB. Dynamic interfacial tension of surfactant solutions. Adv Colloid Interface Sci 2017;247:115–29.

[45] Ferri JK, Stebe KJ. Which surfactants reduce surface tension faster? A scaling argument for diffusion-controlled adsorption. Adv Colloid Interface Sci 2000;85:61–97.
[46] Eggleton CD, Stebe KJ. An adsorption–desorption- controlled surfactant on a deforming droplet. J Colloid Interface Sci 1998;208:68–80.
[47] Jin F, Balasubramaniam R, Stebe KJ. Surfactant adsorption to spherical particles: the intrinsic length scale governing the shift from diffusion to kinetic-controlled mass transfer. J Adhesion 2004;80:773–96.
[48] Mucic N, Javadi A, Kovalchuk NM, Aksenenko EV, Miller R. Dynamics of interfacial layers-experimental feasibilities of adsorption kinetics and dilational rheology. Adv Colloid Interface Sci 2011;168:167–78.
[49] Mikati N, Wall S. Diffusion of sodium dedecyl sulfate studied by a steady-state technique. Langmuir. 1993;9:113–6.
[50] Alvarez NJ, Walker LM, Anna SL. Diffusion-limited adsorption to a spherical geometry: the impact of curvature and competitive time scales. Phys Rev E Stat Nonlin Soft Matter Phys 2010;82:011604.
[51] Luo ZY, Shang XL, Bai BF. Effect of soluble surfactant on the motion of a confined droplet in a square microchannel. Phys Fluids 2019;31.
[52] Kiratzis I, Kovalchuk NM, Simmons MJH, Vigolo D. Effect of surfactant addition and viscosity of the continuous phase on flow fields and kinetics of drop formation in a flow-focusing microfluidic device. Chem Eng Sci 2022;248.
[53] Dukhin SS, Kovalchuk VI, Gochev GG, Lotfi M, Krzan M, Malysa K, et al. Dynamics of rear stagnant cap formation at the surface of spherical bubbles rising in surfactant solutions at large Reynolds numbers under conditions of small Marangoni number and slow sorption kinetics. Adv Colloid Interface Sci 2015;222:260–74.
[54] Pesci C, Weiner A, Marschall H, Bothe D. Computational analysis of single rising bubbles influenced by soluble surfactant. J Fluid Mech 2018;856:709–63.
[55] Langevin D, Monroy F. Marangoni stresses and surface compression rheology of surfactant solutions. Achievements and problems. Adv Colloid Interface Sci 2014;206:141–9.
[56] Fainerman VB, Kovalchuk VI, Aksenenko EV, Miller R. Dilational viscoelasticity of adsorption layers measured by drop and bubble profile analysis: reason for different results. Langmuir. 2016;32:5500–9.
[57] Lucassen J, van den Tempel M. Dynamic measurements of dilational properties of a liquid interface. Chem Eng Sci 1972;27:1283–91.
[58] Hosokawa S, Hayashi K, Tomiyama A. Evaluation of adsorption of surfactant at a moving interface of a single spherical drop. Exp Thermal Fluid Sci 2018;96:397–405.
[59] Levich VG. Physicochemical hydrodynamics. New Jersey: Prentice-Hall; 1962.
[60] Eastoe J, Dalton JS. Dynamic surface tension and adsorption mechanisms of surfactants at the air-water interface. Adv Colloid Interface Sci 2000;85:103–44.
[61] He Y, Yazhgur P, Salonen A, Langevin D. Adsorption-desorption kinetics of surfactants at liquid surfaces. Adv Colloid Interface Sci 2015;222:377–84.
[62] Lunkenheimer K, Miller R. A criterion for judging the purity of adsorbed surfactant layers. J Colloid Interface Sci 1987;120:176–83.
[63] Alvarez NJ, Lee W, Walker LM, Anna SL. The effect of alkane tail length of CiE8 surfactants on transport to the silicone oil-water interface. J Colloid Interface Sci 2011;355:231–6.
[64] Alvarez NJ, Vogus DR, Walker LM, Anna SL. Using bulk convection in a microtensiometer to approach kinetic-limited surfactant dynamics at fluid-fluid interfaces. J Colloid Interface Sci 2012;372:183–91.
[65] Fainerman VB, Kovalchuk VI, Aksenenko EV, Ravera F, Liggieri L, Loglio G, et al. A multistate adsorption model for the adsorption of C14EO4 and C14EO8 at the solution/air interface. Colloids Interf 2021:5.
[66] Ritacco H, Langevin D, Diamant H, Andelman D. Dynamic surface tension of aqueous solutions of ionic surfactants: role of electrostatics. Langmuir. 2011;27:1009–14.
[67] Fernandez J, Krechetnikov R, Homsy GM. Experimental study of a surfactant-driven fingering phenomenon in a Hele-Shaw cell. J Fluid Mech 2005;527:197–216.
[68] Li B, Geeraerts G, Joos P. Kinetic equations for transfer-controlled adsorption kinetics. Colloids Surf A Physicochem Eng Asp 1994;88:251–66.
[69] Hsu CT, Shao MJ, Lin SY. Adsorption kinetics of C12E4 at the air-water interface: adsorption onto a fresh interface. Langmuir. 2000;16:3187–94.
[70] Pan R, Green J, Maldarelli C. Theory and experiment on the measurement of kinetic rate constants for surfactant exchange at an air/ water interface. J Colloid Interface Sci 1998;205:213–30.
[71] Lin SY, Tsay RY, Lin LW, Chen SI. Adsorption kinetics of C12E8 at the air-water Interface: adsorption onto a clean interface. Langmuir. 1996;12:6530–6.
[72] Kumar N, Couzis A, Maldarelli C. Measurement of the kinetic rate constants for the adsorption of superspreading trisiloxanes to an air/aqueous interface and the relevance of these measurements to the mechanism of superspreading. J Colloid Interface Sci 2003;267:272–85.
[73] Narayan S, Moravec DB, Dallas AJ, Dutcher CS. Droplet shape relaxation in a four-channel microfluidic hydrodynamic trap. Phys Rev Fluids 2020:5.
[74] Xu JH, Li SW, Lan WJ, Luo GS. Microfluidic approach for rapid interfacial tension measurement. Langmuir. 2008;24:11287–92.
[75] Kim P, Kwon KW, Park MC, Lee SH, Kim SM, Suh KY. Soft lithography for microfluidics: a review. Biochip J 2008;2:1–11.
[76] Utada AS, Fernandez-Nieves A, Stone HA, Weitz DA. Dripping to jetting transitions in coflowing liquid streams. Phys Rev Lett 2007;99:094502.
[77] Stone HA. Dynamics of drop deformation and breakup in viscous fluids. Annu Rev Fluid Mech 1994;26:65–102.
[78] Anna SL, Mayer HC. Microscale tipstreaming in a microfluidic flow focusing device. Phys Fluids 2006;18.
[79] Utada AS, Fernandez-Nieves A, Gordillo JM, Weitz DA. Absolute instability of a liquid jet in a coflowing stream. Phys Rev Lett 2008;100:014502.
[80] Kovalchuk NM, Sagisaka M, Steponavicius K, Vigolo D, Simmons MJH. Drop formation in microfluidic cross-junction: jetting to dripping to jetting transition. Microfluidics Nanofluidics 2019;23.
[81] Li X-B, Li F-C, Yang J-C, Kinoshita H, Oishi M, Oshima M. Study on the mechanism of droplet formation in T-junction microchannel. Chem Eng Sci 2012;69:340–51.
[82] Cubaud T, Mason TG. Capillary threads and viscous droplets in square microchannels. Phys Fluids 2008;20.
[83] van Hoeve W, Dollet B, Versluis M, Lohse D. Microbubble formation and pinch-off scaling exponent in flow-focusing devices. Phys Fluids 2011;23.
[84] Moyle TM, Walker LM, Anna SL. Predicting conditions for microscale surfactant mediated tipstreaming. Phys Fluids 2012;24.
[85] Jeong WC, Lim JM, Choi JH, Kim JH, Lee YJ, Kim SH, et al. Controlled generation of submicron emulsion droplets via highly stable tip-streaming mode in microfluidic devices. Lab Chip 2012;12:1446–53.
[86] Taylor GI. The formation of emulsions in definable fields of flow. Proc Royal Soc London A 1934;146:501–23.
[87] Herrada MA, Ponce-Torres A, Rubio M, Eggers J, Montanero JM. Stability and tip streaming of a surfactant-loaded drop in an extensional flow. Influence of surface viscosity. J Fluid Mech 2022:934.
[88] Kovalchuk NM, Roumpea E, Nowak E, Chinaud M, Angeli P, Simmons MJH. Effect of surfactant on emulsification in microchannels. Chem Eng Sci 2018;176:139–52.
[89] Kalli M, Angeli P. Effect of surfactants on drop formation flow patterns in a flow-focusing microchannel. Chem Eng Sci 2022;253.
[90] Garstecki P, Fuerstman MJ, Stone HA, Whitesides GM. Formation of droplets and bubbles in a microfluidic T-junction-scaling and mechanism of break-up. Lab Chip 2006;6:437–46.
[91] van Steijn V, Kleijn CR, Kreutzer MT. Predictive model for the size of bubbles and droplets created in microfluidic T-junctions. Lab Chip 2010;10:2513–8.
[92] Christopher GF, Noharuddin NN, Taylor JA, Anna SL. Experimental observations of the squeezing-to-dripping transition in T-shaped microfluidic junctions. Phys Rev E Stat Nonlin Soft Matter Phys 2008;78:036317.
[93] Xu JH, Li SW, Tan J, Luo GS. Correlations of droplet formation in T-junction microfluidic devices: from squeezing to dripping. Microfluidics Nanofluidics 2008;5:711–7.
[94] Wang K, Zhang L, Zhang W, Luo G. Mass-transfer-controlled dynamic interfacial tension in microfluidic emulsification processes. Langmuir. 2016;32:3174–85.
[95] Kalli M, Chagot L, Angeli P. Comparison of surfactant mass transfer with drop formation times from dynamic interfacial tension measurements in microchannels. J Colloid Interface Sci 2022;605:204–13.
[96] Xu JH, Dong PF, Zhao H, Tostado CP, Luo GS. The dynamic effects of surfactants on droplet formation in coaxial microfluidic devices. Langmuir. 2012;28:9250–8.
[97] Wang K, Lu YC, Xu JH, Luo GS. Determination of dynamic interfacial tension and its effect on droplet formation in the T-shaped microdispersion process. Langmuir. 2009;25:2153–8.
[98] Ma S, Sherwood JM, Huck WTS, Balabani S. On the flow topology inside droplets moving in rectangular microchannels. Lab Chip 2014;14.
[99] Jakiela S, Korczyk PM, Makulska S, Cybulski O, Garstecki P. Discontinuous transition in a laminar fluid flow: a change of flow topology inside a droplet moving in a micron-size channel. Phys Rev Lett 2012;108:134501.
[100] Oishi M, Kinoshita H, Fujii T, Oshima M. Simultaneous measurement of internal and surrounding flows of a moving droplet using multicolour confocal micro-particle image velocimetry (micro-PIV). Measure Sci Technol 2011;22.
[101] Kinoshita H, Kaneda S, Fujii T, Oshima M. Three-dimensional measurement and visualization of internal flow of a moving droplet using confocal micro-PIV. Lab Chip 2007;7:338–46.
[102] Mießner U, Helmers T, Lindken R, Westerweel J. μPIV measurement of the 3D velocity distribution of Taylor droplets moving in a square horizontal channel. Exp Fluids 2020;61.
[103] Song H, Tice JD, Ismagilov RF. A microfluidic system for controlling reaction networks in time. Angew Chem Int Ed Engl 2003;42:768–72.
[104] Liu Z, Li M, Pang Y, Zhang L, Ren Y, Wang J. Flow characteristics inside droplets moving in a curved microchannel with rectangular section. Phys Fluids 2019;31.
[105] Olgac U, Muradoglu M. Effects of surfactant on liquid film thickness in the Bretherton problem. Int J Multiphase Flow 2013;48:58–70.
[106] Mulligan MK, Rothstein JP. The effect of confinement-induced shear on drop deformation and breakup in microfluidic extensional flows. Phys Fluids 2011;23.
[107] Wu Y, Fu T, Zhu C, Wang X, Ma Y, Li HZ. Shear-induced tail breakup of droplets (bubbles) flowing in a straight microfluidic channel. Chem Eng Sci 2015;135:61–6.
[108] Atasi O, Haut B, Pedrono A, Scheid B, Legendre D. Influence of soluble surfactants and deformation on the dynamics of centered bubbles in cylindrical microchannels. Langmuir. 2018;34:10048–62.
[109] Liu Z, Zhang L, Pang Y, Wang X, Li M. Micro-PIV investigation of the internal flow transitions inside droplets traveling in a rectangular microchannel. Microfluidics Nanofluidics 2017;21.
[110] Kashyap S, Almutairi Z, Qin N, Zhao P, Bedi S, Johnson D, et al. Effects of surfactant size and concentration on the internal flow fields of moving slug and disk-like droplets via μ-PIV. Chem Eng Sci 2022;255.
[111] Helmers T, Kemper P, Thöming J, Mießner U. The flow topology transition of liquid–liquid Taylor flows in square microchannels. Exp Fluids 2022;63.

[112] Guzman AR, Kim HS, de Figueiredo P, Han A. A three-dimensional electrode for highly efficient electrocoalescence-based droplet merging. Biomed Microdevices 2015;17:35.
[113] Narayan S, Makhnenko I, Moravec DB, Hauser BG, Dallas AJ, Dutcher CS. Insights into the microscale coalescence behavior of surfactant-stabilized droplets using a microfluidic hydrodynamic trap. Langmuir. 2020;36:9827–42.
[114] Liu Z, Wang X, Cao R, Pang Y. Droplet coalescence at microchannel intersection chambers with different shapes. Soft Matter 2016;12:5797–807.
[115] Shenoy A, Rao CV, Schroeder CM. Stokes trap for multiplexed particle manipulation and assembly using fluidics. Proc Natl Acad Sci U S A 2016;113:3976–81.
[116] Schroën K, de Ruiter J, Berton-Carabin C. The importance of interfacial tension in emulsification: connecting scaling relations used in large scale preparation with microfluidic measurement methods. ChemEngineering. 2020:4.
[117] Steegmans ML, Warmerdam A, Schroen KG, Boom RM. Dynamic interfacial tension measurements with microfluidic Y-junctions. Langmuir. 2009;25:9751–8.
[118] Chagot L, Quilodran-Casas C, Kalli M, Kovalchuk NM, Simmons MJH, Matar OK, et al. Surfactant-laden droplet size prediction in a flow-focusing microchannel: a data-driven approach. Lab Chip 2022;22:3848–59.
[119] van der Graaf S, Schroen CG, van der Sman RG, Boom RM. Influence of dynamic interfacial tension on droplet formation during membrane emulsification. J Colloid Interface Sci 2004;277:456–63.
[120] MacLeod CA, Radke CJ. Surfactant exchange kinetics at the air/water interface from the dynamic tension of growing liquid drop. J Colloid Interface Sci 1994;166:73–88.
[121] Kovalchuk NM, Vollhardt D. Marangoni instability and spontaneous non-linear oscillations produced at liquid interfaces by surfactant transfer. Adv Colloid Interface Sci 2006;120:1–31.
[122] Wang X, Riaud A, Wang K, Luo G. Pressure drop-based determination of dynamic interfacial tension of droplet generation process in T-junction microchannel. Microfluid Nanofluid 2015;18:503–12.
[123] Lan W, Wang C, Guo X, Li S, Luo G. Study on the transient interfacial tension in a microfluidic droplet formation coupling interphase mass transfer process. AIChE J 2016;62:2542–9.
[124] Lan W, Wang Z, Wang M, Liu D, Guo X, Sun Q, et al. Determination of transient interfacial tension in a microfluidic device using a Laplace sensor. Chem Eng Sci 2019;209.
[125] Pinczewski WV. The formation and growth of bubbles at a submerged orifice. Chem Eng Sci 1981;36:405–11.
[126] Javadi A, Krägel J, Pandolfini P, Loglio G, Kovalchuk VI, Aksenenko EV, et al. Short time dynamic interfacial tension as studied by the growing drop capillary pressure technique. Colloids Surf A Physicochem Eng Asp 2010;365:62–9.
[127] Zhang X, Harris MT, Basaran OA. Measurement of dynamic surface tension by a growing drop technique. J Colloid Interface Sci 1994;168:47–60.
[128] Zhao C-X, Rondeau E, Cooper-White JJ, Middelberg APJ. Microfluidic elucidation of the effects of interfacial rheology on droplet deformation. Indust Eng Chem Res 2011;51:2021–9.
[129] Goel S, Joshi N, Uddin MS, Ng S, Acosta E, Ramachandran A. Interfacial tension of the water-diluted bitumen interface at high bitumen concentrations measured using a microfluidic technique. Langmuir. 2019;35:15710–22.
[130] Narayan S, Moravec DB, Hauser BG, Dallas AJ, Dutcher CS. Removing water from diesel fuel: understanding the impact of droplet size on dynamic interfacial tension of water-in-fuel emulsions. Energy Fuel 2018;32:7326–37.